Computation & theory

Atomistic insight into three-dimensional twin embryo growth in Mg alloys

Yang Hu[1] and Dennis M. Kochmann[1,*] (iD)

[1] *Mechanics and Materials Lab, Department of Mechanical and Process Engineering, ETH Zurich, 8092 Zurich, Switzerland*

ABSTRACT

Magnesium (Mg) alloys are essential for industrial applications but poorly understood from a mechanistic perspective, while a comprehensive understanding of their mechanical behavior can guarantee a more efficient alloy design as well as a greater application potential. As one of the key deformation mechanisms in Mg and Mg alloys, twinning is investigated in this work. Molecular dynamics simulations are used to perform a systematic study of the effect of alloying elements and solute compositions on twin embryo growth in nine Mg alloys. The alloying elements include Al, Zn, Li, Ca, Pb, Nd, Ce, Sn, and Y, covering a wide range of element properties such as lattice constant, bulk/shear modulus, and cohesive energy. We demonstrate a faster migration of the dark side than the bright side of twin embryos in both pure Mg and Mg alloys. All solute atoms tested in this work exhibit a pinning effect on the motion of twin facets on the dark side. The motion of facets on the bright side, particularly twin boundaries, can be accelerated by solutes. Therefore, the majority of solutes can reduce the velocity difference between the dark side and the bright side of the twin. The overall twin embryo growth is restricted in most alloys except Mg–Y, Mg–Li and Mg–Nd with certain solute concentrations. Our results present important insight for tailoring twin structures and hence the mechanical properties of Mg alloys.

GRAPHICAL ABSTRACT
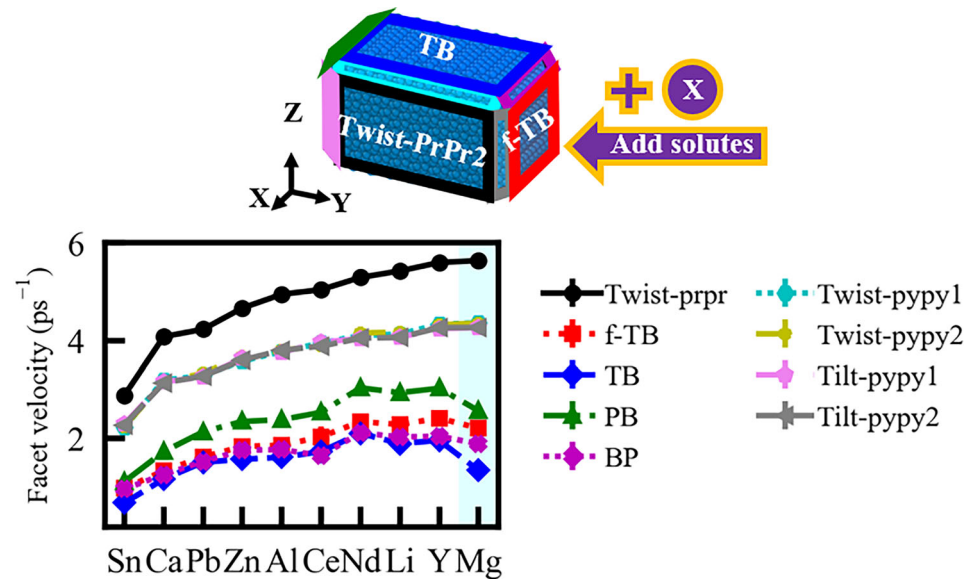
Introduction

Magnesium (Mg) is the lightest metal with a high application potential in the aerospace, automobile, and biomedical industries [1, 2]. The mechanical performance of Mg and its alloys, particularly the strength and ductility, in response to external loads remains an interesting research topic. Twinning is a commonly observed deformation mode in Mg and Mg alloys, which could largely accommodate plastic strains together with the easily activated basal slips [3, 4]. The widely reported twin modes include tension twins $\{10\bar{1}2\}\langle\bar{1}011\rangle$ and $\{11\bar{2}1\}\langle\bar{1}\bar{1}26\rangle$, formed by stretching the c-axis, and contraction twins $\{10\bar{1}1\}\langle10\bar{1}2\rangle$ and $\{11\bar{2}2\}\langle11\bar{2}3\rangle$, formed by compressing the c-axis [5]. Among all twin modes that have been found so far, $\{10\bar{1}2\}$ tension twins are the most profuse ones in plastically deformed Mg and Mg alloys. Some polycrystalline pure Mg samples only require applied stresses as low as 4 MPa for such twins to be initiated [6], still being higher than the critical resolved shear stress for activating basal slips but much lower than that for activating prismatic and pyramidal slip systems [7–9]. $\{10\bar{1}2\}$ twins

can grow into large sizes and consume the entire parent structure. It is essential to engineer or design optimal twin structures to achieve desired properties of Mg and Mg alloys. For example, Chen et al. [10] managed to produce fine-grained AZ31 alloy samples with high twin density using dynamic extrusion at room temperature. Such samples exhibit higher yield strength and strain to failure than fine-grained samples with low twin density, and the fracture surfaces exhibit more ductile than brittle features. By using surface SPEX milling (SSM), Wang et al. [11] created pure Mg samples with varying density of twin meshes (intersecting arrays of twins) and realized a higher ultimate tensile strength and a twofold increase in ductility.

Twin structures reported in the literature, including optical micrographs, transmission electron microscopy (TEM) images, or electron backscattered diffraction (EBSD) images, are usually displayed using 2D projections from a particular perspective. Most twins exhibit similar features, i.e., lamellar shapes with relatively sharp twin tips [12–15]. At a higher resolution, one can identify the coherent twin boundaries (TBs) [16], basal-prismatic and prismatic-basal interfaces (BPs and PBs, respectively) [17], and sometimes forward twin boundaries (f-TBs), which

are close to perpendicular to primary TBs [18, 19]. These interfaces separate the twinned region from the matrix. Atomistic simulations are typically set up according to the twin structure observed in experiments to study the motion of individual interfaces or the overall growth of a twin embryo [20–22]. Simulations show structural features formed on TBs, twinning disconnections, defined as interfacial dislocations with a step height of twice the interplanar spacing of the twin plane. The motion of TBs is achieved by the constant nucleation and glide of twinning disconnections [23–25]. Various disconnection types are also found on other interfaces and play an essential role in interface motion and overall twin embryo growth. For example, Zu et al. [26, 27] show that one-layer disconnections ($c/2$, where c is the lattice parameter of Mg) are generated on BP/PB interfaces, and two of them can be transformed into one twinning disconnection at the intersection of the TB and BP/PB planes.

Only in recent years has it been found that the twin morphology cannot be fully described by 2D projections, which only show the twin structure parallel to the twin shear (also called the "bright side" view according to Liu et al. [28]). By compressing Mg AZ31 alloys along the RD, Fernández et al. [29] found secondary and tertiary $\{10\bar{1}2\}$ twins (with low Schmid factors) of irregular shapes in 3D, meaning that twin thickness measurements based on 2D twin lamella are not enough to determine the true twin size or to study twin growth. At the atomic scale, Liu et al. [28] first managed to characterize the so-called "dark side" of a twin embryo, i.e., the twin structure observed along the twinning direction. Wang et al. [30] reported the interfaces or twin facets that bound the twin on the dark side, including twist-pyramidal pyramidal planes (Twist-pypy1), twist-prismatic prismatic planes (Twist-prpr2), and tilt-pyramidal pyramidal planes (Tilt-pypy1). Each of these planes is differently oriented with different interfacial energies, atomic structures, and migration behaviors. Through MD simulations, Gong et al. [31] found that Twist-prpr2 planes move the fastest among all facets and, therefore, twin growth along the dark side is much more rapid than the growth along the bright side. While Liu et al. [28] observed misfit dislocations with screw characters on relaxed Twist-prpr2 facets, the migration of such facets occurs via atomic shuffle combined with the lateral glide of screw misfit

dislocations [28]. Such misfit dislocations impose a pinning effect on the motion of Twist-prpr2 facets and cause irregular twin shapes on the dark side.

The motion of twin facets and the overall twin growth can be tuned by alloying elements [4, 16, 32–37]. Prior investigations highlighted the segregation of solute atoms to particular twin facets, such as coherent TBs and BP/PBs [16, 34, 35, 38], and the segregated solutes were shown to exhibit a strong pinning effect on facet motion [16]. Yet, for the newly reported facets appearing on the dark side of the twin, an understanding of their motion in the presence of alloying elements is still lacking. More importantly, a major downside of most simulations regarding the solute effect on twin facet energy and motion is that individual interfaces are considered. However, at an early twin growth stage, the different twin facets are connected, and their collective motion differs from that of individual, isolated interfaces [31]. Therefore, discussing the motion of certain twin facets that form a twin embryo requires considering them as a part of the boundary that separates the twinned region from the matrix. Numerous experimental studies have studied the mechanical response of Mg alloys to external loading, which naturally takes the 3D twin morphology into account [4, 37, 39–41]. However, it is usually hard to isolate the alloying effect on twin nucleation, twin growth, and slip activities in experiments, unless twinning is the dominant deformation mode [4, 37]. Yet, as the lattice orientation changes during twinning, the initial sample orientation (unfavorable for slip activities) also changes, and inevitably, dislocation slip occurs [4]. Furthermore, it is hard to capture the twin growth kinetics in experiments due to the rapid expansion of twins at an early growth stage. Atomistic simulations can fill this gap and provide detailed information. The majority of simulation works studying the 3D twin morphology at the atomic scale focus on pure Mg [31, 42–44], while the alloying effect on facet motion has been neglected. Alloying elements are usually considered to induce the nucleation of disconnections but harden the migration [36, 45]. The net effect could vary drastically for different disconnection types, leading to diverse migration behavior of the different twin facets. It remains unclear whether solutes slow down or accelerate all twin facets mentioned above, or if certain solutes reduce the motion of some facets but enhance the motion of others, which eventually leads to either an increase or

a decrease in the velocity difference between facets appearing on the bright side and those appearing on the dark side of the twin. Moreover, for solid solutions with randomly distributed solute atoms, the event of a disconnection being pinned by a solute atom, or a disconnection being nucleated with a solute atom's assistance, is rather stochastic than deterministic. Open questions exist about how disconnection nucleation and glide are affected by increasing solute concentration, and the effect of solute concentration levels on the migration of different twin facets. Finally, with the possibility of diverse migration behavior of twin facets, what is the effect of solutes on the growth of twin embryos as a whole?

To provide insight into the early stage twinning behavior in the presence of solute atoms, we conducted molecular dynamics (MD) simulations that investigate the twin embryo growth in nine Mg–X alloys under constant shear stress, considering a 3D twin morphology. The studied alloying elements include Al, Zn, Li, Ca, Pb, Nd, Ce, Sn, and Y. Twin embryos, also referred to as "twin nuclei" [46, 47], exist during the early stages of a twin—after nucleation and before mature twins of several hundred nanometers or micrometers. The difference between a twin embryo and a mature twin also lies in the boundary that separates the twin and the matrix. As mentioned earlier, twin embryos are bound by various twin facets. In contrast, mature twins have TBs as their primary boundaries, since the fast-migrating facets intersect at grain boundaries and vanish [48].

The remainder of this work is structured as follows. In Sect. Methods, we describe the setup of our MD simulations, including the initial twin embryo configuration, the applied solute concentrations, and shear stresses. Section Results first discusses the twin embryo growth in pure Mg to serve as a comparison for the results of alloys. The time evolution of the twin extension along different axes is analyzed, and twin facet velocities are estimated. Next, the solute effect on the motion of individual twin facets, the velocity difference between facets, and the overall twin embryo growth are discussed. Section Discussion explores possible factors contributing to the solute-dependent differences in twinning behavior in alloys. The correlation between facet velocities and the shear modulus and atomic volume mismatch is probed, and the energetic barriers associated with twinning are also estimated. Finally, in Sect. Conclusions, we conclude twinning in alloys and discuss future prospects.

Methods

MD simulations were performed using the large-scale atomic/molecular massively parallel simulator (LAMMPS) package [49]. The $\{10\bar{1}2\}$ tension twin was selected as a model twin mode for investigating the twinning behavior. A schematic of the simulation box is shown in Fig. 1a. The X-axis of the simulation box is set to be along the $[1\bar{2}10]$-direction (a-axis), the Y-axis is along the $[10\bar{1}1]$-direction (twinning direction), and the Z-axis is nearly along the twin plane normal (nearly perpendicular to the $(\bar{1}012)$ plane). The dimensions of the simulation box are $\sim 50 \times \sim 50 \times \sim 50$ nm^3, and the whole box contains $\sim 5{,}500{,}000$ atoms. A twinned region was inserted at the center of the simulation box via the Eshelby method [22]. The initial twin embryo configuration was obtained by structurally relaxing the box under $\sim 7\%$ applied shear strain. The pre-applied shear strain is essential to avoid the shrinkage of the twinned region. The dimensions of the initial twin embryo are ~ 4 nm along the X-axis, ~ 7.4 nm along the Y-axis, and ~ 4 nm along the Z-axis. A detailed description of the construction of the initial simulation configuration can be found in Section S1. Figure 1b–e shows the initial twin embryo from different perspectives. TBs, f-TBs, and BP/PBs usually appear in the bright side view of the twin embryo, with BP/PB interfaces being at about 45° from TBs. The dark side view of the twin embryo shows the Twist-pypy1 and Twist-prpr2 facets, while Tilt-pypy1 facets appear in the view of the twin embryo along the twin plane normal. The Twist-prpr2 facets are at $\sim 90°$ from the horizontal TBs, and Twist-pypy1 facets are at $\sim 50°$ from Twist-prpr2 facets. Tilt-pypy1 facets are at $\sim 40°$ from Twist-prpr2 facets. Figure 1d–e also shows two sets of Tilt-pypy1 and Twist-pypy1 facets with different orientations, similar to the BPs and PBs. In this study, Tilt-pypy1 and Twist-pypy1 are used to address both sets of facets. Small triangular planes connecting the Twist-pypy1 and Tilt-pypy1 facets are shown in Fig. 1b. Such planes are not discussed in this study due to the difficulty of identifying them.
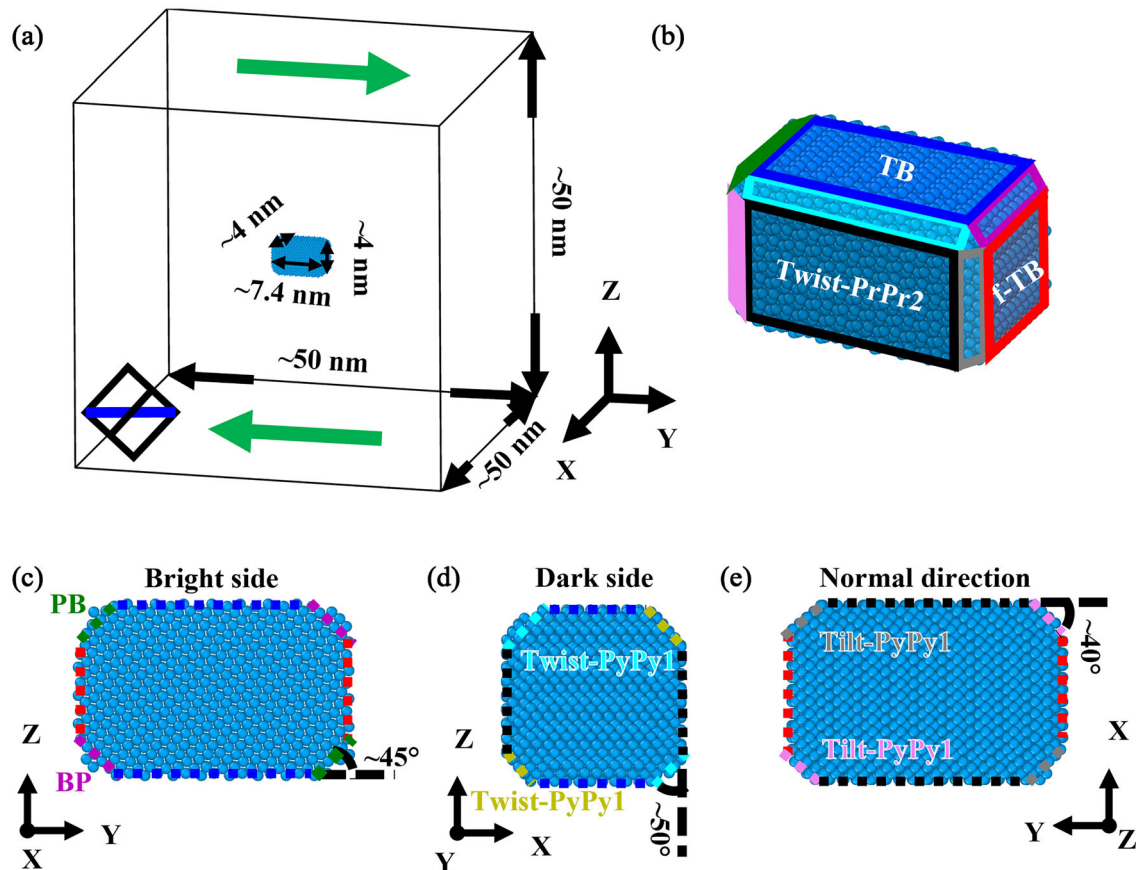
Figure 1 **a** Setup of the MD simulation of twin embryo growth. The green arrows on the top and bottom surfaces indicate the direction of the applied shear stress. **b** Perspective view of the initial twin embryo configuration after structural relaxation. The boundary that separates the twin and the matrix is a combination of TBs, f-TBs, BP/PB planes, Twist-pypy1, Twist-prpr2, and Tilt-pypy1 facets. The initial twin embryo configuration is shown as viewed from **c** the X-axis, **d** the Y-axis, and **e** the Z-axis. The twin facets that are visible from each perspective are marked.

In our study, the growth of a single twin embryo was simulated. Nine alloying elements, Al, Zn, Li, Ca, Pb, Nd, Ce, Sn, and Y, were introduced into the pure Mg samples by randomly replacing Mg atoms. The alloying elements have been reported to alter the microstructure of Mg alloys, to modify mechanical properties such as strength and ductility, corrosion behavior, and solidification behavior [4, 37–41, 45, 50, 51]. Alloying elements also differ in many properties, such as the lattice constant, bulk/shear modulus, and cohesive energy. Thus, our work covers a wide range of alloy properties, allowing for a systematic exploration of the possible effects of solute atoms. Three solute concentrations, 1 at.%, 4 at.%, and 10 at.%, were applied to explore the impact of concentration on facet migration, and they were chosen to represent the range from lightly to heavily alloyed Mg up to the solubility limit. Five simulation runs with different solute distributions were performed for the same alloy to gain statistics on the facet migration behavior. For simulations on pure Mg, five different initial velocity distributions were chosen.

A constant shear stress parallel to the twin plane (XY-plane) was applied to activate twin embryo growth. Shear stresses ranging from 1.2 to 1.6 GPa were used, in which 1.2 GPa is the minimum shear stress required to trigger twin growth in pure Mg with current initial conditions (considering the simulation box size and initial twin embryo size), while shear stresses lower than 1.2 GPa lead to either no growth or shrinkage of the embryo. Atoms were relaxed under an NPT (isothermal-isobaric) ensemble at 1 K, with the temperature adjusted every 100 time steps with one integration step of 0.1 fs. The low temperature, 1 K, was used to avoid any effect of

thermal fluctuations on twin growth, making it easier to identify the key deformation mechanisms. Such low temperatures are common for simulations of twin growth [15, 21, 22, 28, 42–44]. The modified embedded-atom method (MEAM) potentials developed by Kim et al. [52–55], Jang et al. [56], and Lee et al. [57] were used to describe the atomic interactions in Mg alloys (Mg [52], Mg–Li [53], Mg–Y [54], Mg–Sn [54], Mg–Nd [55], Mg–Pb [55], Mg–Al [56], Mg–Zn [56], Mg–Ca [56], and Mg–Ce [57]). These potentials were developed based on the same unary potential for Mg. Structural visualization is performed using the Open Visualization Tool (OVITO) [58]. To differentiate the twin from the matrix, the polyhedral template matching method [59] was used to characterize the local crystalline structure and orientation associated with each atom in the system, which can be encoded as an orientation quaternion, $q = q_w + q_x i + q_y j + q_z k$. Component q_x presents a good criterion regardless of alloy type, simulation timestep, and applied stress (see Fig. S2, where the twinned region is dark blue, while the matrix is red). The twin extension along each axis was approximated by the difference between the maximum and minimum positions of the twin along that axis. For "tilted" facets, such as BP/PB, Twist-pypy1, and Tilt-pypy1 facets, the simulation box was first rotated, so these facets became perpendicular to one of the coordinate axes, and the twin extension could be measured as described above. The velocity of each facet was estimated by fitting the variation of the twin extension with time using a linear regression fit.

Results

Twin facet motion in pure Mg

We first review the facet motion in pure Mg simulations conducted at different shear stresses, serving later as a reference for the simulations of alloys. Figure 2 presents 2D projections of the twin structure at 10 ps in a simulation with 1.6 GPa applied shear stress. To show the facets that are hidden inside the box, a 1-nm-thick slab at the center of the simulation box is taken for viewing the twin structure from each perspective. The red twin tips appear along the X-axis, signaling the dark side of the twin embryo, where the Twist-prpr2 planes move the fastest, while facets on the bright side, such as the horizontal TBs

and f-TBs, move more slowly and are shown in green. Compared with the initial twin embryo structure, TBs and f-TBs are more curved, while interfaces that move faster are relatively straight and are of smaller interfacial area. Magnified views of selected twin facets are shown in Figs. 2d–e along with part of the twinned region and the matrix. In Fig. 2d–f, the twinning disconnections formed on horizontal TBs, f-TBs, and one-layer disconnections formed on BP/PB interfaces are observed. Viewing from the X-axis (see Fig. 3), we find that the majority of twinning disconnections are nucleated at the intersections of TBs with BP/PBs. Thus, it requires more time for twinning disconnections to travel from one side of the plane to the other if the interfacial area is larger, in turn contributing to a lower facet velocity in the direction of the plane normal. However, this 2D projection only shows the motion of twinning disconnections along the twinning direction, i.e., the Y-axis. The expansion of twinning disconnections along the X-axis is shown in the set of frames in light green boxes. Twinning disconnections first appear at the center of the TB plane and start expanding to the intersections with Twist-pypy1 planes. The curved TBs could be considered as multiple twinning disconnections stacking on one another. The curved f-TBs (Fig. 2c) also indicate the stacking of twinning disconnections on such planes. Braisaz et al. [18] as well as Lay and Nouet [19] found interfacial dislocations with Burgers vectors roughly equal to four twinning dislocations and seven twinning dislocations on the f-TB. In our previous work on the twin embryo growth in pure Mg using a 2D configuration [60], the Burgers vector of a twinning disconnection formed on the f-TB was identified with the same magnitude as the twinning disconnections formed on the horizontal TB (b_t). No disconnections with large Burgers vectors (nb_t, where n is a large integer) were observed. In experiments, the expansion of the twin embryo along the twinning direction allows the f-TBs to interact with point defects or lattice dislocations, which may contribute to forming interfacial dislocations with large Burgers vectors. In our simulations, the twin embryo starts with defect-free interfaces, and no other defects are introduced into the simulation box. For the newly observed Twist-prpr2 facets, Liu et al. [28] reported theoretically the existence of misfit dislocations of screw character on fully relaxed facets. On the contrary, our starting twin configuration is obtained under a certain amount of applied
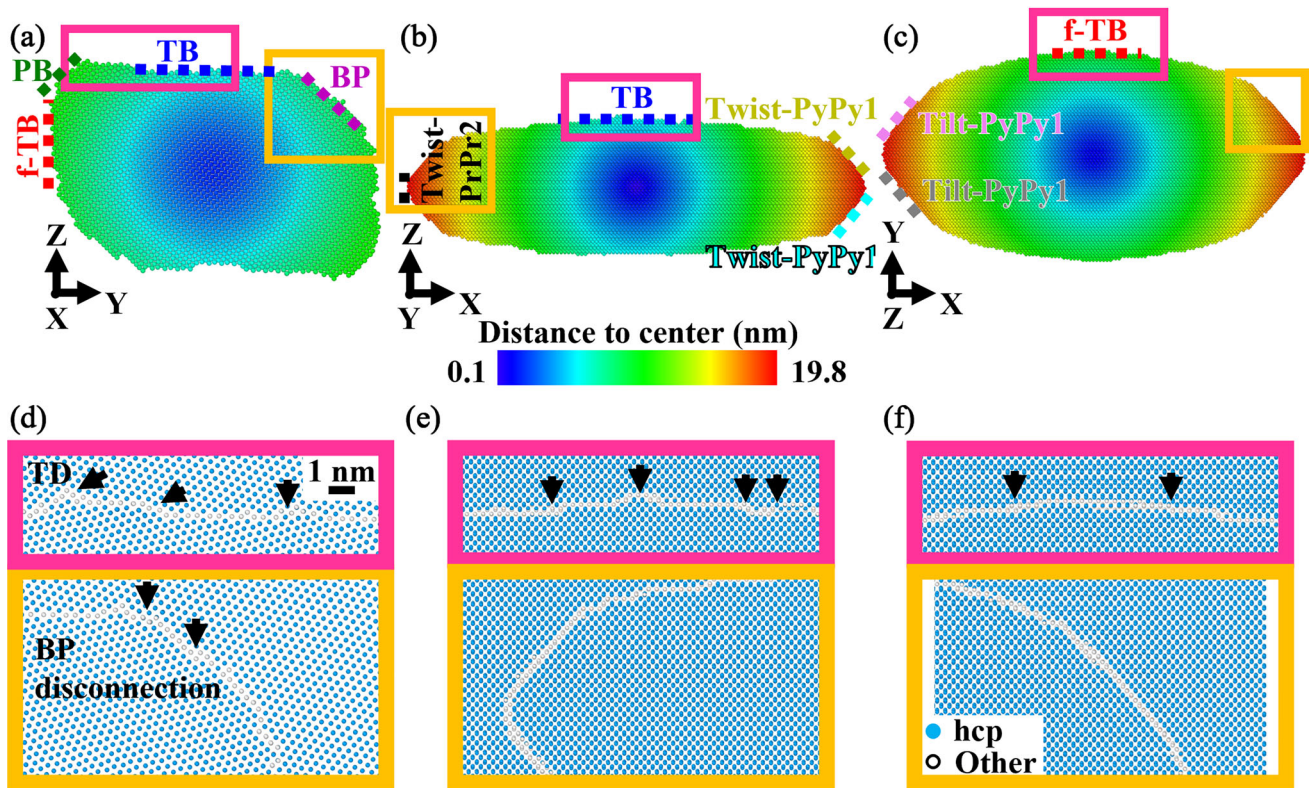
Figure 2 Twin embryo configuration at 10 ps viewed along the **a** X-axis, **b** Y-axis, and **c** Z-axis in a simulation performed at 1.6 GPa shear stress. Atoms are colored according to their distance from the center of the twin embryo, dark blue atoms are closer to the center, while red atoms are far away from the center. **d**–**f** Magnified views of disconnections formed on different facets (marked by black arrows). The pink and yellow boxes in **a**–**c** indicate where the magnified views are taken. Atoms are colored using the structural type, light blues atoms are Mg, and white atoms are atoms on the boundaries that separate the twin from the matrix.

shear strains, so the twin facets are initially stressed. During the embryo growth process, Twist-prpr2 facets move fast and maintain small interfacial areas, and there is no observation of misfit dislocations.

The migration of Twist-pypy1 and Tilt-pypy1 planes is observed to happen layer by layer, as shown in Fig. 4. The top frames display the atomic structure of one Twist-pypy1 plane viewed along the Y-axis between 9.7 and 9.9 ps. The plane slightly expands as time progresses (dark blue) and reaches its new position (light green) at 9.9 ps. The atoms at the initial plane position join the twinned region and are identified as hcp atoms. To determine the migration mechanism of Twist-pypy1 planes, the atomic snapshots of the same interface from 9 ps (dark blue) to 9.9 ps (red) are stacked on top of each other to show the displacements of atoms, see the last frame of Fig. 5. The atoms close to the new position of the Twist-pypy1 plane first undergo an upward displacement (shear displacement), followed by atomic

shuffling displacements which bring them to their final positions. For atoms near the intersections of Twist-pypy1 and TBs or the intersections of Twist-pypy1 and Twist-prpr2 facets, the atomic displacements are not the same as those right in front of the Twist-pypy1 planes. At the intersections of different planes, more complex defects may exist and be involved in the transformation of disconnections on different twin facets. For example, Barret and El Kadiri [26] reported disclinations (line defects that violate rotational symmetry) at the intersections of TBs and BP/PBs. In the MD work of Wan et al. [44], 3D twin growth in pure Mg was studied by applying tensile strains on a $20 \times 20 \times 20$ nm^3 simulation box with a strain rate of 1×10^9 s^{-1}. The authors reported a pure shuffle-dominated motion of Twist-pypy1 facets, which we attribute to the different twin sizes. With a $20 \times 20 \times 20$ nm^3 simulation box size, the twin size in their work is significantly smaller (see Fig. 8 and Fig. 10 in [44]), and it is usually hard to
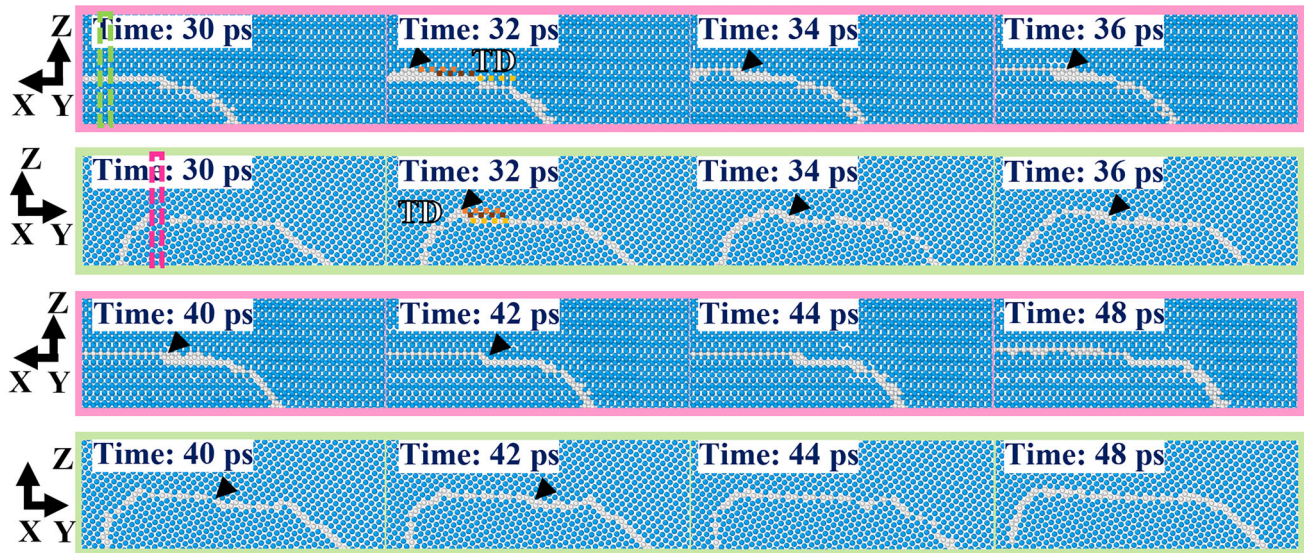
Figure 3 Motion of one twinning disconnection on the upper twin boundary viewed from the Y-axis (frames in pink boxes) and the X-axis (frames in light green boxes). 1-nm slabs are shown to indicate the atomic structure of the upper twin boundary, and the dashed rectangles in the frames at 30 ps show the location of the slab. Black arrows mark the location of the disconnection front. The short orange, brown, and yellow dashed lines in the second and sixth frames show the positions of the same three atomic planes from two different perspectives.

capture the formation and glide of disconnections on small interfaces, especially for those with fast motion. The migration mechanism of an interface might also change with its size. A dual-step nucleation of $\{10\bar{1}2\}$ twins was previously observed [21, 61]. A small group of atoms first undergo a basal-prismatic transformation via pure atomic shuffling, and this small, reoriented region is bound by BP/PB interfaces. TBs are then formed by the accumulation of disconnections on BP/PB interfaces, and, in a later growth stage, the formation and glide of twinning disconnections are observed. In this work, we skip the twin nucleation process by directly inserting a twin embryo inside the simulation box, and with the initial twin size and pre-applied strains, TBs are already stable and appear after structural relaxation. The size of the twin reaches about $39.5 \times 20 \times 13.1$ nm^3, when the displacements of atoms around Twist-pypy1 planes are measured.

The fast migration of Twist-prpr2 planes is confirmed in Fig. 6, in which the twin dimensions along different axes are plotted against time. Facet velocities are estimated by fitting the time evolution of twin dimensions using linear regression. Note that the facet velocity is half the slope of the fitting line (the increase of the twin extensions is the sum of position changes of both planes along that direction).

Figure 6a shows the simulation results at 1.6 GPa shear stress. The process of twin embryo growth can be separated into three regimes. During the initial ~ 2 ps of the simulation, there is a slow expansion regime, indicating an incubation period before discernable twin growth starts, which is why the data before 2 ps is discarded in the following estimation of facet velocity. Around 12 ps, Twist-prpr2 planes arrive at the edge of the simulation box. After 12 ps the twin extensions along the other directions continue to increase over time, yet the twin growth now occurs under a 2D condition. (The dark side has been merged with its periodic image.) It is also found that facets on the dark side strongly interact with their periodic images starting from ~ 11 ps, corresponding to the peaks seen around 11 ps in the time evolution of the slope (see Fig. S5(a)). Such a strong interaction is expected to occur when two interfaces get close. Therefore, when estimating the twin facet velocity under a 3D growth condition, the data after 11 ps is discarded. Figure 6b compares the motion of different twin facets. Twist-prpr2 migrates with the maximum velocity, followed by Twist-pypy1 and Tilt-pypy1, which are connected to Twist-prpr2, while horizontal TBs are the slowest interfaces. Our finding is consistent with what was reported by Gong et al. [31]. As mentioned earlier, Twist-prpr2 facets in
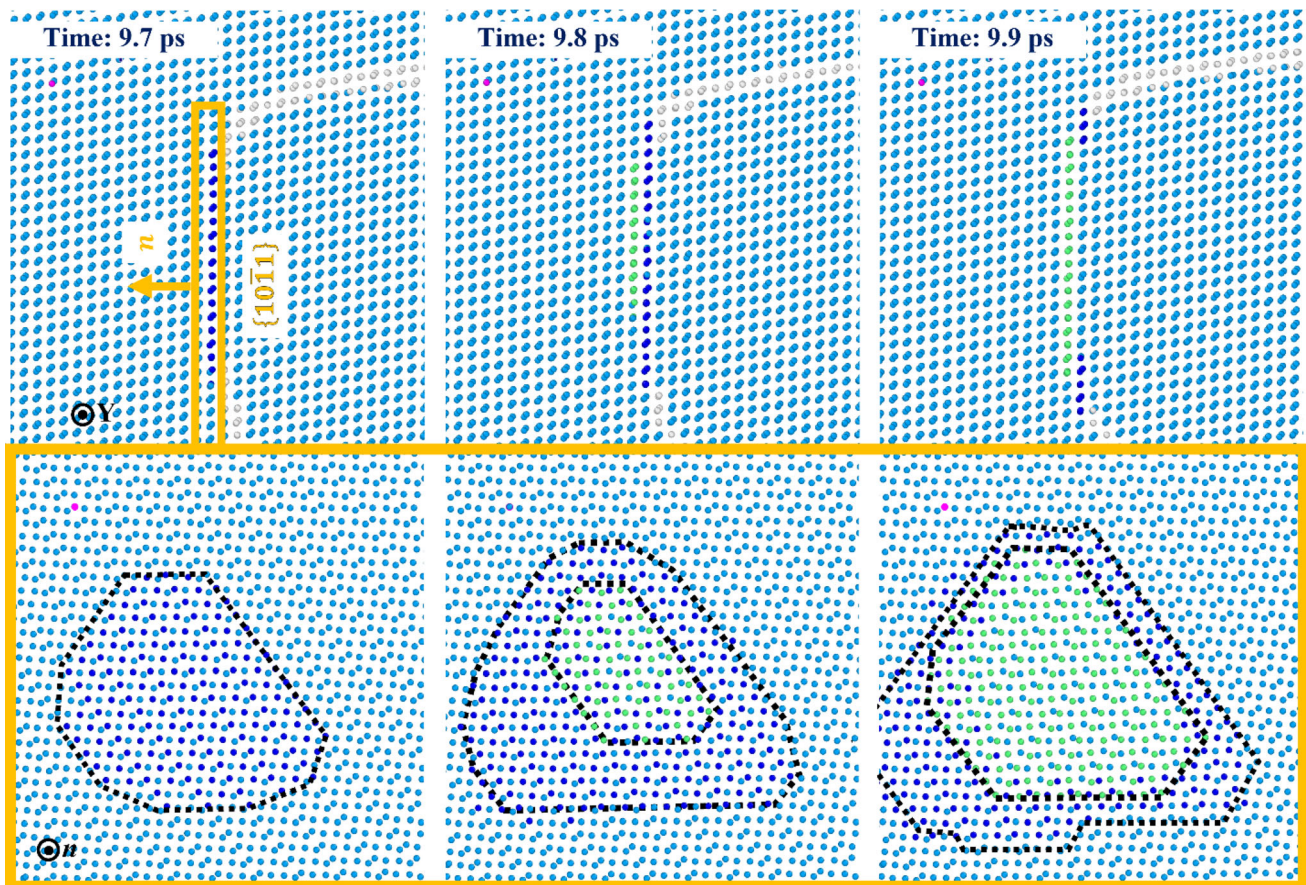
Figure 4 Motion of one Twist-pypy1 plane viewed along the *Y*-axis (top frames) and the plane normal (lower frames). The atoms on the boundary in two atomic planes are colored using dark blue (the initial position of the Twist-pypy1 plane) and light green (the new position). The dotted lines in the lower frames mark the previous and new Twist-pypy1 plane that bound the twin embryo. Magenta atoms in each frame are reference atoms.

our simulation do not contain misfit dislocations. We note that Liu et al. [28] observed such interfacial dislocations when using a larger twin embryo in simulations (12 nm along the TB normal direction) and via fully relaxing the boundary. The existence of misfit dislocations could place a pinning effect on the motion of Twist-prpr2 and reduce its velocity. Comparing twin facet velocities at different applied shear stresses, it is found that for low shear stresses such as 1.2 GPa and 1.3 GPa, there is limited growth of the bright side. The velocities of TBs, f-TBs, and BP/PBs are almost zero. From 1.2 GPa to 1.25 GPa shear stress, there is a strong increase in the velocity of the dark side. Beyond 1.3 GPa shear stress, the increase in shear stress places less effect on fast facets, i.e., Twist-prpr2, Twist-pypy1, and Tilt-pypy1. Yet, the difference in velocities is more noticeable for slower facets, which are TBs, f-TBs, and BP/PBs. The velocities of facets on the bright side in the 2D growth

stage are summarized in Section S3. One additional simulation with almost twice the box dimensions along the *X*-axis was performed to demonstrate the rather small influence of the simulation boxes size on the results, as shown in Section S4.

Due to the high shear stresses and low simulation temperatures, the facet velocities in our work reach the order of magnitude of 10^3 m s^{-1}, some of which are higher than the velocities of elastic shear and longitudinal waves traveling in bulk Mg [62]. Transonic and supersonic dislocations were reported previously by Gumbsch and Gao [63], who simulated dislocation nucleation and motion in W by mimicking an indentation process. Such dislocations were created at a strong stress concentration and soon reached speeds that surpassed the speed of sound. In our simulations, interfacial dislocations formed on different twin facets were observed, such as the twinning dislocations on TBs (Fig. 2), and the
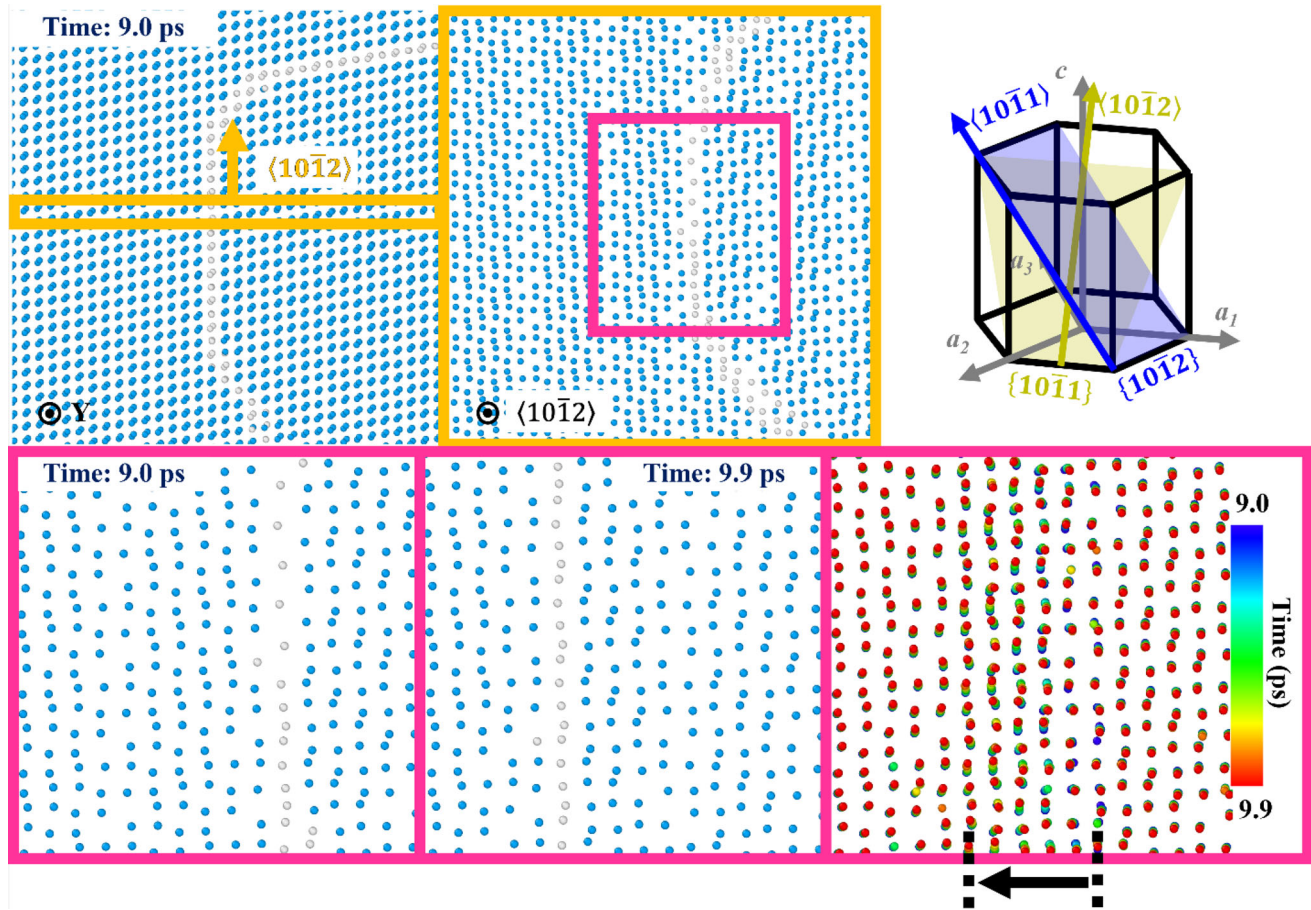
Figure 5 Atomic structure of one Twist-pypy1 plane viewed along the $\langle 10\overline{1}2 \rangle$-direction, and the atomic displacements from 9 to 9.9 ps. The third frame in the first row shows the orientation of the Twist-pypy1 facet and TB in an Mg unit cell. In the last frame, atoms are colored according to time, with dark blue atoms appearing early and red atoms appearing later. Note that some atoms are missing because a ~ 0.45 nm slab is taken to show the atomic structure around the Twist-pypy1 plane, and some atoms fall out of the slab as the facet migrates. Dashed lines mark the positions of the Twist-pypy1 plane at 9 and 9.9 ps, with the black arrow showing the direction of motion. The pink and yellow boxes show where the slabs of materials are taken for visualization.

dislocations formed on the Twist-pypy1 planes (Fig. 5). These dislocations drive the motion of the twin interfaces, and therefore twin facets could reach a high speed. Experimental evidence of fast-moving twin facets can be found in the work of Kannan et al. [64], who investigated twin dynamics in Mg single crystals, using in situ ultra-high-speed optical imaging. Specimens were loaded in compression, and $\{10\overline{1}2\}$ tension twins were nucleated at stresses of 5–7 MPa. The twin tips (referred to as f-TBs here) of the first generation of twins were found to propagate at speeds on the order of 1 km s^{-1}. Note that instead of focusing on the absolute value of twin facet velocities obtained in simulations, we here focus on the difference in facet motion between various Mg alloys.

To understand the different migration behaviors of twin facets in pure Mg, the 2D spatial distribution of the shear stress for one simulation conducted at 1.6 GPa is shown in Fig. 7. In each frame, the matrix exhibits large positive shear stresses (orange areas), while the stresses within the twin are relaxed (green and blue areas at the center). This confirms that the twin grows at the expense of the applied shear stresses. At 10 ps, the small regions in front of the Twist-prpr2 planes show the highest shear stress. Facets tend to propagate toward the regions with large shear stresses, which helps explain the fast propagation of Twist-prpr2 planes. These high shear stresses in front of the Twist-prpr2 planes are eventually released through the merging of the twin with its periodic images. The regions outside of horizontal
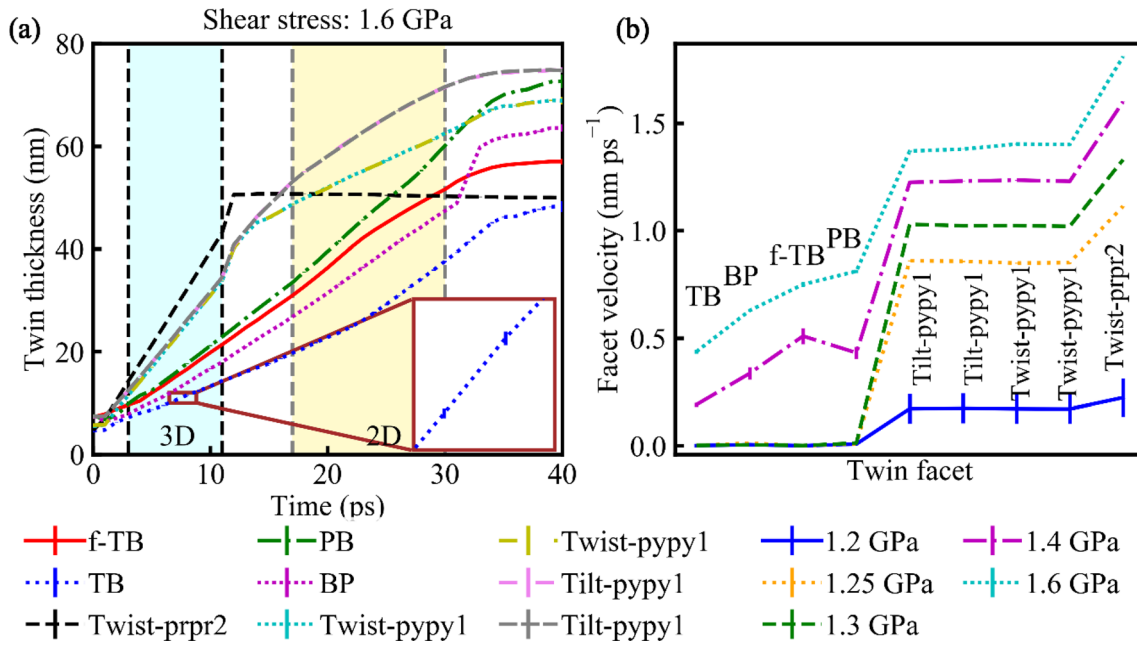
Figure 6 a Variation in twin extensions with time. The inset shows a small segment of the twin thickness along the Z-axis versus time to highlight the error bars. The error bars of the twin thicknesses are small and barely visible in **a** due to the large span of curves. **b** Facet velocities obtained at different shear stresses (1 nm ps^{-1} = 1 km·s^{-1}).
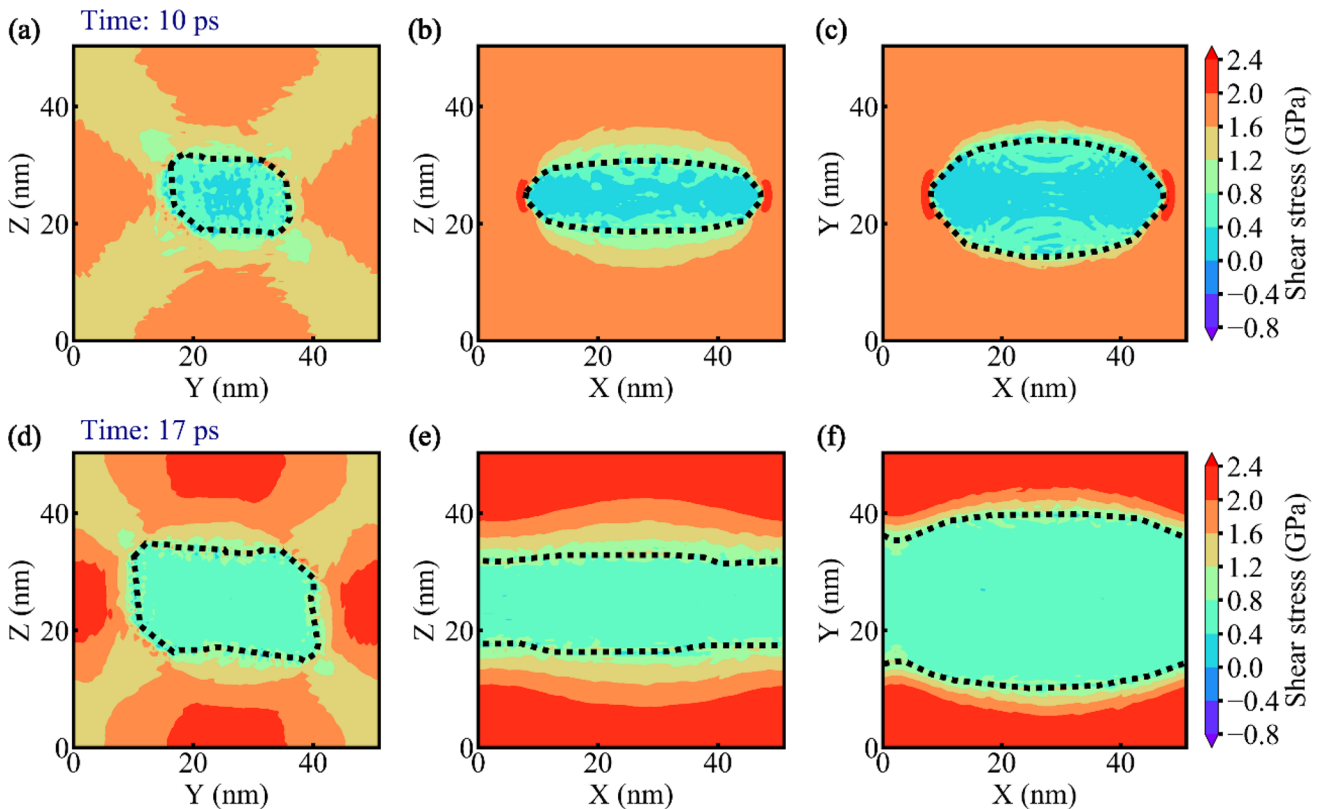

Figure 7 Two-dimensional spatial distribution of the shear stress within the **a** YZ-, **b** XZ-, and **c** XY-planes at 10 ps and **d-f** at 17 ps. The simulation is performed at 1.6 GPa shear stress. Dotted lines in each frame mark the boundaries that separate the twin and the matrix, drawn according to the twin configuration at 10 and 17 ps.

TBs and f-TBs exhibit a transition in color, from green to yellow, showing a stress transition zone between the twin and matrix far away from the boundary. The shear stress of the twinned region drops to near-zero values and may even become locally negative near the TBs after the twinning deformation occurs due to the stress reversal induced by the twinning shear transformation [65–67]. Comparing the shear stress distributions at 10 ps (3D growth stage) and 17 ps (2D growth stage), it is found that the regions in front of TBs and the f-TBs show higher shear stresses (red instead of orange) under 2D growth conditions, corresponding to the faster motion of twin facets on the bright side at the 2D growth stage.

In summary, results for pure Mg show a faster migration of the dark side of the twin embryo, with Twist-prpr2 facets being the fastest among all, while the horizontal TBs are the slowest. In the bright side view of a TB, twinning disconnections are formed at the intersections of the TB and BP/PBs and then migrate toward the other side, while the dark side view displays an expansion of twinning disconnections toward the intersections of the TB and Twist-pypy1 facets. The propagation of Twist-pypy1 and Tilt-pypy1 facets are realized by atomic shear and shuffling displacements. Finally, the spatial distribution of shear stresses shows regions of large shear stresses located in front of fast-moving twin facets.

Twin facet motion in Mg alloys

The growth of the twin embryo in Mg alloys is again described by the variation of twin extensions along different axes over time, as shown in Fig. S6. Two factors contribute to the different twin extensions measured for alloy samples. First, the twin facet velocities are different in different alloys (the faster the facet velocity in an alloy, the larger the obtained twin extensions). The second factor is the varying lattice constants of alloys (the larger the lattice constant of a certain alloy, the larger the measured twin extensions). The contribution of the second factor in twin extensions is generally smaller than that of the first. However, to better compare the facet migration and overall twin growth between different alloys, the original values of twin extensions are normalized by the lattice constants, a, of alloys with the same alloying elements and solute concentrations. Details about calculating the lattice constant of alloys can be found in Section S6. In Mg alloys, twin facets become

rougher due to the interactions with solute atoms during their motion. With different solute distributions, the locations where disconnections are formed and when a disconnection migration is pinned by solutes differ, resulting in larger statistical variations (and hence error bars) than for pure Mg in the measurement of twin extensions. In general, the twin embryo growth in alloys undergoes a similar process as in pure Mg. It starts with a slow expansion regime, followed by a steady 3D twin growth stage. The Twist-prpr2 planes reach the edge of the simulation box first. After that the dark side of the twin embryo disappears, and twin growth enters the 2D stage. The obtained facet velocities are plotted against each other in Fig. 8. The results of TB, BP, Twist-pypy1, and Twist-prpr2 are shown as examples. The three data points for pure Mg represent simulations conducted at 1.3, 1.4, and 1.6 GPa shear stress. In Fig. 8a, the velocities of Twist-pypy1 and Twist-prpr2 exhibit a close to a linear trend. Twist-pypy1 facets are directly connected to Twist-prpr2 facets, which could contribute to the linear relationship between the two facet velocities. The fact that the data points of pure Mg lie on the same line as those of the alloys shows that the impact of introducing solute additions is similar to the impact of shear stress on the motion of the dark side. Consequently, the velocity of one facet can be predicted by knowing the velocity of the other facet. Figure 8b shows that although data points of different alloys and pure Mg exhibit an increasing trend (i.e., the faster motion of Twist-prpr2 means a faster motion of TB), the data points are more scattered, signaling a drastically different solute effect on the motion of TBs and Twist-prpr2 facets. When plotting the TB velocity vs. the velocity of one facet directly connected to it, such as the BP facet (see Fig. 8c), the trend is close to linear but not as perfect as in Fig. 8a. Yet, it should be noted that these relations between facet velocities are obtained under the loading condition of constant shear stresses. It would be interesting to check whether such relations exist for facet moving under other loading conditions such as constant shear strains.

We proceed to discuss the alloying effect of solutes in the 3D growth stage with regard to the solute effect on (1) the motion of individual facets, (2) the facet motion difference, and (3) the overall twin embryo growth. For all alloying elements and solute concentrations that have been tested, the Twist-prpr2 facets glide with maximum velocities (see Figs. 9a–c),
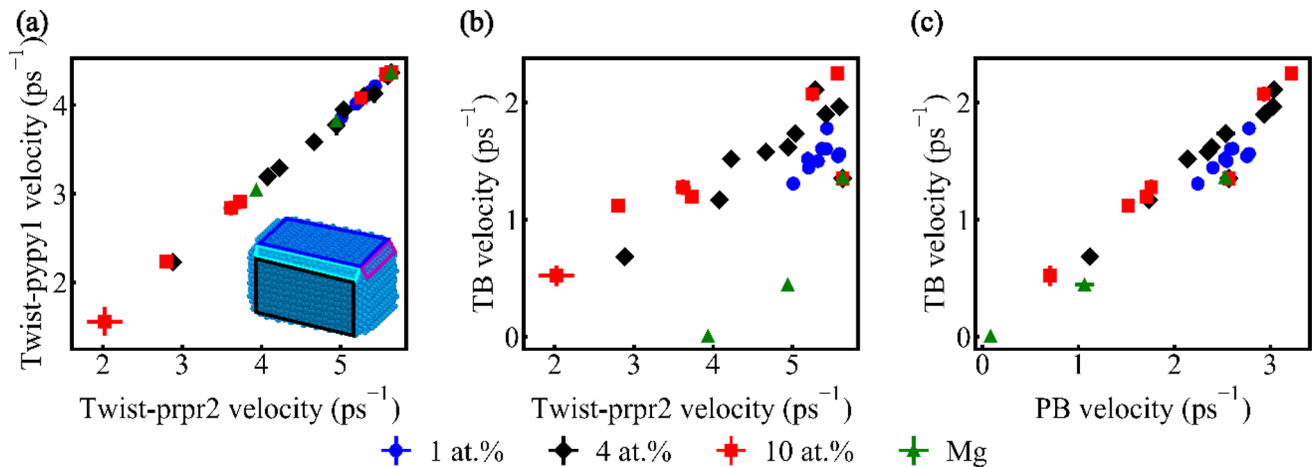
Figure 8 Variation of **a** Twist-pypy1 velocity with Twist-prpr2 velocity, **b** TB velocity with Twist-prpr2 velocity, and **c** TB velocity with PB velocity for pure Mg and alloys with 1 at.%, 4 at.%, and 10 at.% solutes. The inset in **a** shows these facets on the boundary of the twin embryo. The unit of facet velocity is ps^{-1} because the twin extensions are normalized by the lattice constant, a, of different Mg alloys for comparison purposes.

followed by the Twist-pypy1 and Tilt-pypy1 facets directly connected to Twist-prpr2. Among the facets on the bright side, PB planes move faster, while the horizontal TBs are the slowest. Comparing the results of alloys with pure Mg (the rightmost data point on each curve in Fig. 9), it is found that for the dark side of the twin embryo, the velocities of facets migrating in alloys are smaller than those in pure Mg, meaning that solute atoms exhibit a pinning effect and slow down the motion of the dark side. By contrast, certain alloying elements can enhance facet motion on the bright side. For example, almost all alloying elements can increase the motion of the horizontal TB in Mg-4 at.% X alloys, while Ca and Sn slightly decrease the TB velocity. Adding Nd, Y, and Li also increases the motion of other facets on the bright side, while adding Ce helps maintain a similar PB velocity as in pure Mg. For Mg-10 at.% X alloys, only the addition of Li and Y increases the motion of all facets on the bright side. As the concentration increases, fewer element types increase the bright side velocity, likely due to the stronger pinning effect that comes with higher solute concentrations. The motion of the same twin facet in alloys with different solute concentrations is compared in Figs. 9d–f. For Twist-prpr2, Twist-pypy1, and Tilt-pypy1 planes that appear on the dark side (the results for Twist-pypy1 and Tilt-pypy1 facets are shown in Fig. S7), increasing solute concentrations can further reduce the motion of the dark side, while the two elements that do not place a discernable influence are Li and Y. For twin facets on

the bright side, taking the horizontal TB as an example (Fig. 9f), Sn and Ca reduce the facet velocity as the concentration increases from 1 to 4 at.%, while Pb, Zn, Al, and Ce do not exhibit a significant influence on facet motion. On the contrary, Y, Li, and Nd can enhance the facet motion as the concentration increases from 1 to 4 at.%. After the solute concentration reaches 10 at.%, Pb, Zn, Al, and Ca restrict the twin facet motion, while Y and Li atoms are able to further increase the facet motion. Ca decreases the motion of both the dark side and bright side of the twin embryo, and it places a stronger pinning effect on the motion of the facets that move faster than the facets that move more slowly. There also exist solute elements that exhibit an opposite effect on the motion of dark and bright sides, including Y and Li. To quantify the reduction in facet velocity difference, in Fig. 10, the velocity ratio of TB to Twist-prpr2 facet, and the velocity ratio of f-TB to Twist-prpr2 are shown. A velocity ratio smaller than that for pure Mg means the facet motion difference is enhanced by adding solutes and vice versa. Regarding the TB and Twist-prpr2 facets, most solutes reduce the difference in their velocities, and this solute effect becomes stronger as the solute concentration increases, except for Ca and Al. For f-TB and Twist-prpr2 facets, Li, Y, Ce, and Nd reduce the difference in their velocities at all solute concentrations. The effect of Ca, Sn, Al, and Zn changes from reducing facet velocities difference to enhancing facet velocities difference as the solute concentration increases. The change of facet velocity
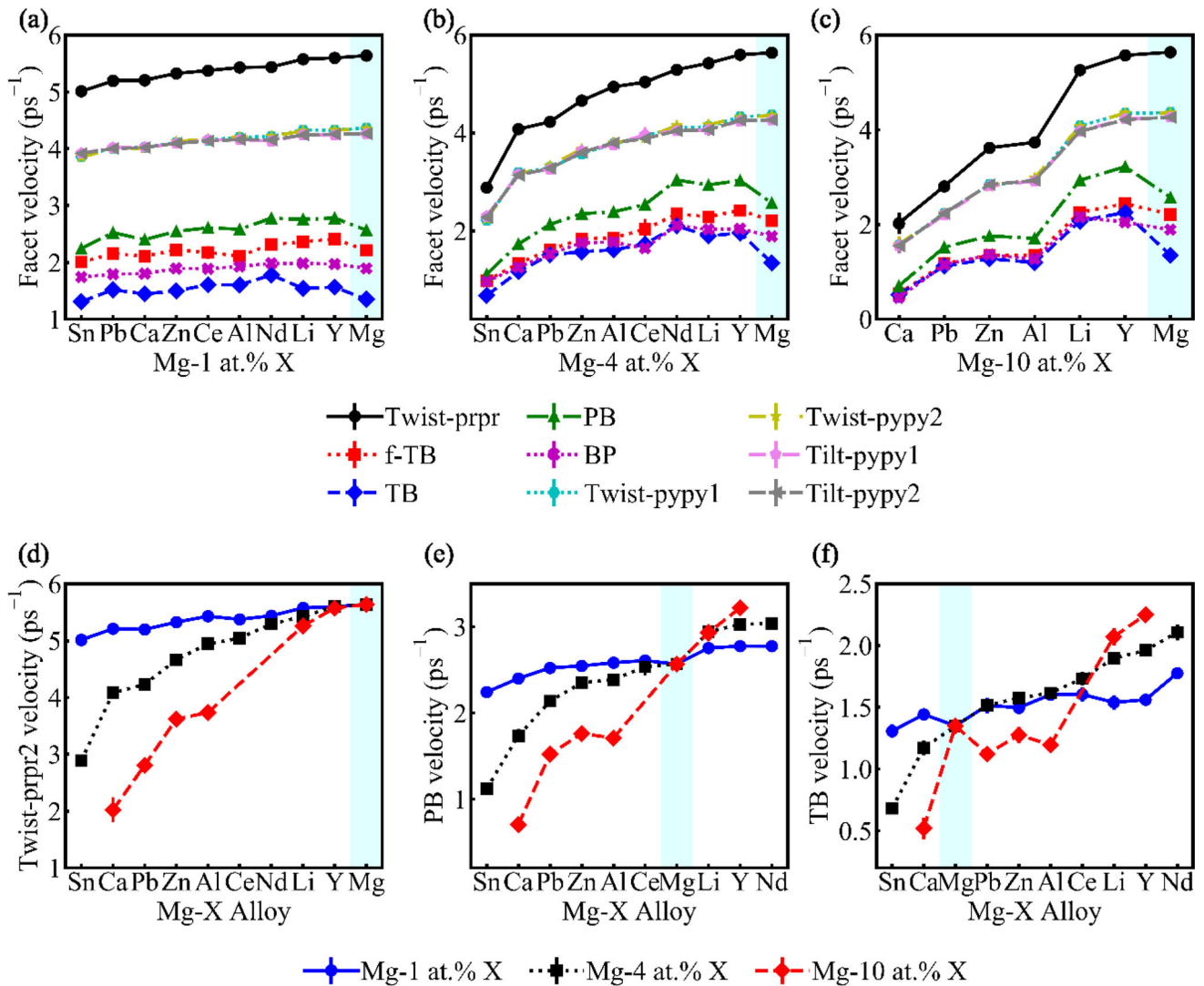
Figure 9 Twin facet velocities for **a** Mg-1 at.% X alloys, **b** Mg-4 at.% X alloys, and **c** Mg-10 at.% X alloys. Data points for different alloys are ordered according to the velocities of Twist-prpr2 facets. The velocity of **d** Twist-prpr2 facet, **e** BP facet, and **f** TB for all alloys are compared. The data points of different alloys are ordered according to the twin facet velocity for Mg-4 at.% X alloys.

ratio also indicates a change of twin shape. In pure Mg, with Twist-prpr2 being the fastest facet, the $l_{TB}/l_{Twist\text{-}prpr2}$ and $l_{f\text{-}TB}/l_{Twist\text{-}prpr2}$ ratios reach 0.33 and 0.50, respectively, near the end of 3D growth stage, while in Mg-4 at.% Nd alloys, in which the facet velocity difference is significantly reduced, $l_{TB}/l_{Twist\text{-}prpr2}$ and $l_{f\text{-}TB}/l_{Twist\text{-}prpr2}$ reach values of 0.45 and 0.56, respectively.

The effect of alloying elements on the overall twin embryo growth is also explored by plotting the variation of twin atomic fractions against time (see Fig. S10). The twin atomic fraction is defined as the number of atoms within the twinned region divided by the total number of atoms in the simulation box,

and the data of alloys is further normalized by the twin atomic fraction for pure Mg at the same time. Therefore, in Figs. 11a–c, a value of 1 represents pure Mg. While a ratio of less than 1 implies a twin embryo size smaller than the embryo size in pure Mg at the same time, a ratio larger than 1 corresponds to a twin embryo with a size larger than that in pure Mg. Figure 11 shows that most alloying elements inhibit the twin embryo growth. Even though certain alloying elements can enhance the motion of individual facets that appear on the bright side, the slower motion of the dark side dominates the overall twin embryo growth and results in smaller twin embryo sizes in the alloys. The exceptions are Mg–Li and Mg–
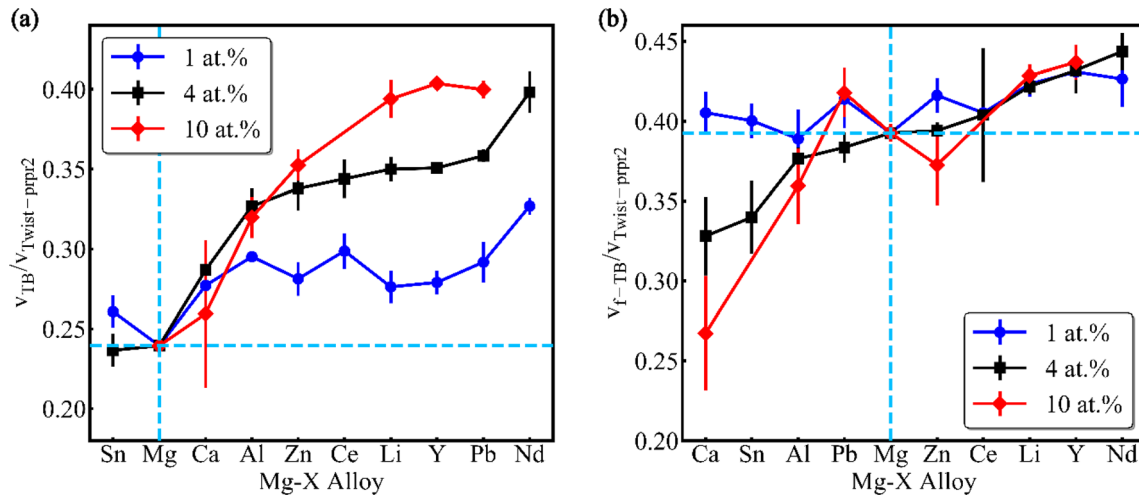
Figure 10 Velocity ratio of **a** the TB to Twist-prpr2 facet, and **b** the f-TB to Twist-prpr2 facet for Mg-1 at.% X, Mg-4 at.% X, and Mg-10 at.% X alloys.
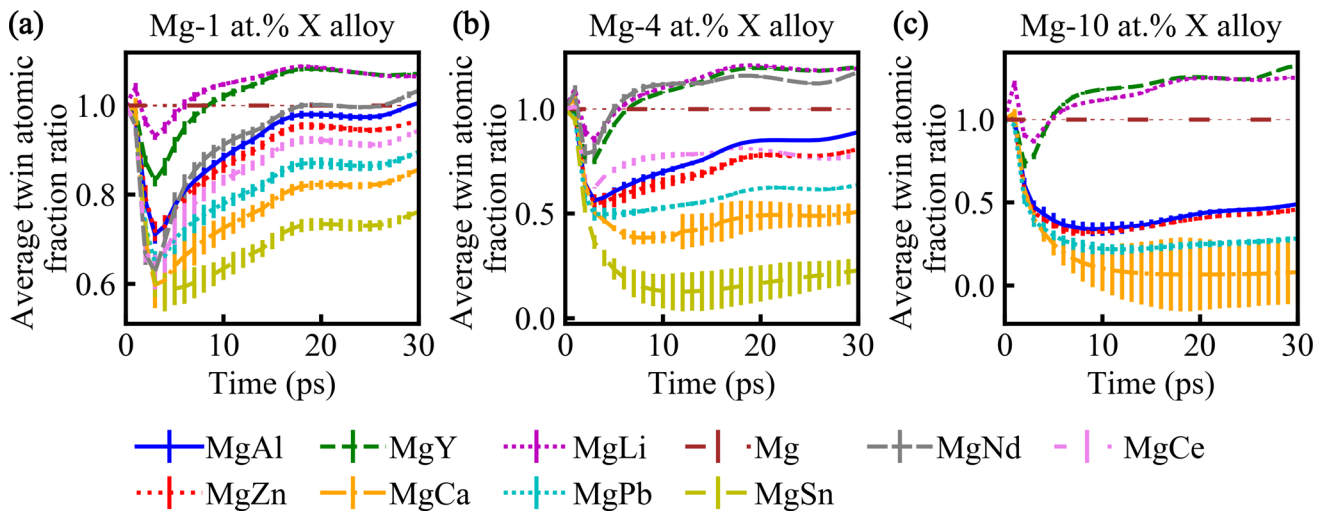

Figure 11 Time evolution of the normalized twin atomic fraction for **a** Mg-1 at.% X alloys, **b** Mg-4 at.% X alloys, **c** Mg-10 at.% X alloys. The twin atomic fraction is defined as the number of atoms in the twinned region divided by the total number of atoms in the simulation box, and the twin atomic fraction ratio is the twin atomic fraction normalized by that of pure Mg.

Y at all three concentration levels and Mg-Nd at 4 at.% concentration. As mentioned above, Li, Y, and Nd do not significantly restrict the motion of the dark side. At the same time, they can even enhance the motion of the bright side, resulting in a faster overall twin embryo growth in alloys than the embryo growth in pure Mg.

Discussion

Our simulations revealed the effects of various solutes on individual twin facet motion and the overall twin embryo growth. All studied solutes reduce the velocities of facets on the dark side of the twin embryo; the higher the solute concentration, the stronger the pinning effect of solute elements. On the contrary, most solutes promote the motion of facets that appear on the bright side, particularly TBs. However, as the solute concentration increases, the pinning effect of solutes becomes dominant, so fewer solute species can promote TB motion. Y and Li

atoms place similar effects on facet motion, regardless of the solute concentration. Li, Y, Ce, Nd solutes decrease the velocity of facets on the dark side while increasing the velocity of facets on the bright side, leading to a decrease in the velocity difference between facets such as TBs and Twist-prpr2. Regarding the overall growth of the twin embryo, Y and Li enhance twin growth at all three tested concentrations, as does 4 at.% of Nd, while all other studied solutes restrict twin growth.

To understand the migration behavior of facets in different alloys, one typically looks at the spatial distribution of shear stresses (e.g., the results for Mg-10 at.% Li and Mg-10 at.% Sn alloys are shown in Section S8). We found that in all alloy simulations, regions of high stresses are distributed randomly due to the random solute atom locations, which is why it is hard to rationalize the facet motion based on the shear stress distribution. Additional simulations were performed on bicrystalline samples containing two TBs or two Twist-prpr2 facets to probe the solute effect on energies associated with twin facet motion, i.e., the time evolution of the potential energy of one solute atom or Mg atom as a twin transformation occurs (computational details are provided in Section S9). TBs and Twist-prpr2 facets were chosen as they are the slowest and fastest twin facets, respectively. There are two different types of lattice sites on $\{10\bar{1}2\}$ planes, due to the corrugated nature of such

planes. The variation of the potential energy of one solute atom or one Mg atom averaged over the atoms located at the same site is shown vs. time in Fig. 12. Note that the potential energies of different solute elements in bulk Mg differ. For easier comparison, from the absolute values of the solute potential energy, we subtracted the time average of the potential energy within the initial 10 ps (this is the potential energy of a solute being in bulk and far from undergoing twin transformation). Among the four solute elements chosen here, Sn and Ca solutes restrict twin growth, while Y and Li enhance twin growth. An Mg atom in bulk must overcome a ∼ 0.04 eV energy barrier as the TB passes by (corresponding to the peak in the curve). Solutes such as Sn, Y, and Li show a similar trend, whereas heavy solute elements (such as Sn and Y) have not reached their final positions in the twin at the end of the simulation (130–150 ps), indicated by nonzero potential energy at the end. For Ca solutes, the curves of potential energy vs. time contain features of strong variations and low-energy states. The results can also be interpreted as follows: the highest energy state of Mg/Y/Li/Sn (or the lowest energy state of Ca) occurs when the atom is about to change from being in the matrix to being in the twin, and such a change of Mg or solute atoms requires them to overcome energy barriers. These energy barriers are estimated in Figs. 12a–b, with Sn and Ca showing the largest
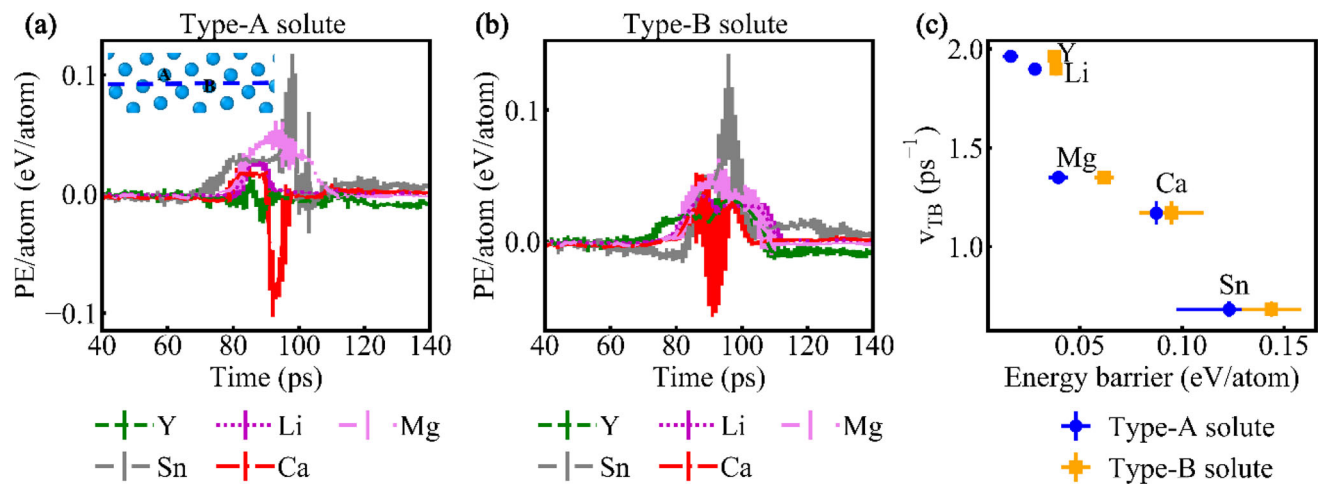

Figure 12 Average potential energy for **a** one type-A solute and **b** one type-B solute vs. time. **c** The velocities of TB facets with energy barriers obtained from **a** and **b**. The inset in **a** shows the atomic structure of corrugated $\{10\bar{1}2\}$ planes. A sites and B sites are differentiated by the local hydrostatic stress as the TB passes by, with A sites being under tension and B sites under compression. Note that for comparing the results of different solutes, the potential energies shown in this figure are the original values subtracted by the potential energy of a solute in the bulk and far from undergoing the twin transformation.

energy barrier. Both solutes exhibit strong pinning effects on facet motion (see Fig. 12c, the TB velocities shown here are obtained from simulations on Mg-4 at.% X alloys). Results for the Twist-prpr2 facet can be found in Section S9. Again, Sn and Ca show the largest energy barrier as the Twist-prpr2 facet passes through. To further compare the effect of Sn and Ca atoms on the twin transformation, the time evolution of the potential energy of a single Sn and Ca atom is plotted along with the atomic structures of the interface before and after it passes by the solute (see Fig. 13). For both Ca and Sn, the formation and glide of nearby twinning disconnections increase their potential energy, followed by a sudden rise or fall. The lowest energy state of Ca occurs when the atom is in the TB, while this is the highest energy state for Sn. This suggests that, even though both Ca and Sn place strong restrictions on TB motion, Sn prevents the TB from approaching, while Ca traps the TB and prevents it from escaping from the solutes. Note that we only aimed for a qualitative comparison of the energy barriers for different solutes instead of having quantitatively accurate data. The latter can be obtained from Nudged Elastic Band (NEB) calculations.

We further explore correlations between facet velocities and specific solute element properties as well as alloy properties. Typical solute element properties associated with the twinning behavior in Mg alloys include the atomic volume mismatch, bond energy, and segregation energy, while alloy properties include the elastic moduli (e.g., measured by the shear modulus). The atomic volume mismatch defines the difference in the size of a solute atom from an Mg atom. A smaller atomic volume mismatch is expected to lead to a twin facet velocity closer to that in pure Mg. Figure 14a shows that Nd has the largest atomic volume mismatch with Mg, while Li is the closest to the atomic volume of Mg. The shear modulus is defined as the linear relation between shear stress and shear strain in the elastic limit. A larger shear modulus means higher stresses are required to deform the material, leading to a lower facet velocity at the same applied shear stress. As shown in Fig. 14b, adding Al, Pb, and Sn atoms increase the shear modulus of the alloy, while other solute atoms decrease the shear modulus of the alloy. Similar trends are observed for all solute concentrations. The data of Mg-4 at.% X alloys are used for exploring the correlation of facet velocities and materials/solute properties. For alloys with 1 at.%
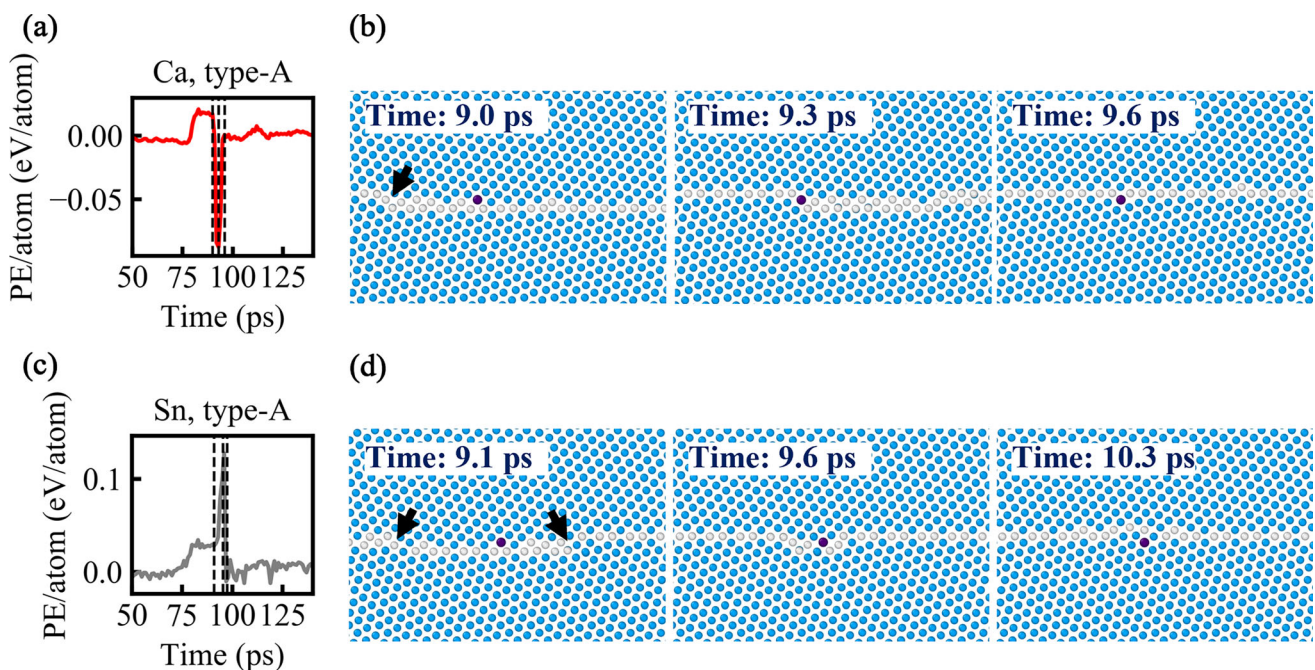

Figure 13 Potential energy for **a** one type-A Ca solute at different times. **b** The atomic structure of the TB, as it passes through the type-A Ca solute. The potential energy for **c** one type-A Sn solute at different times. **d** The atomic structure of the TB as it passes through the type-A Sn solute.
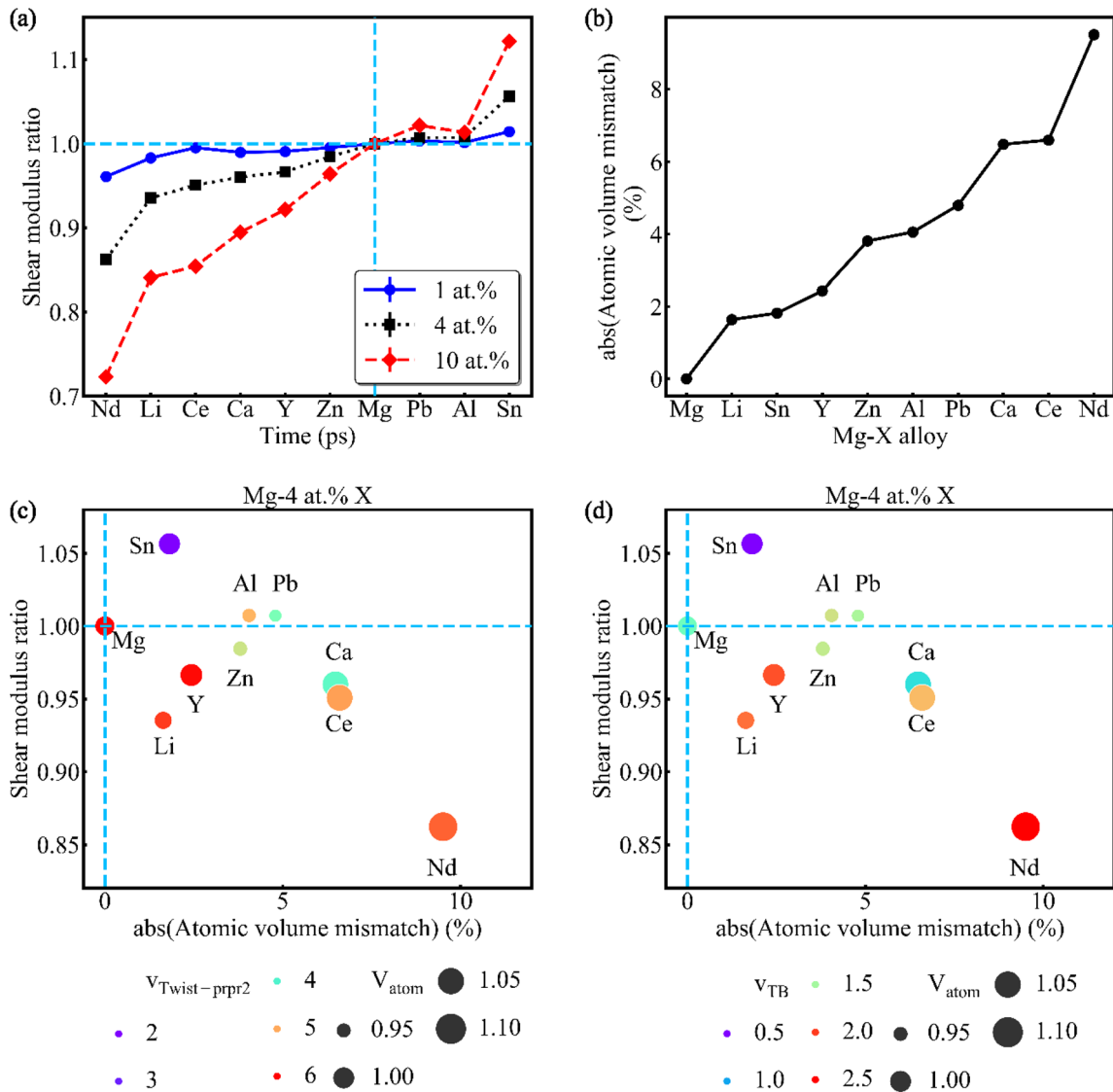
Figure 14 a Shear modulus ratio of Mg alloys with different solutes and solute concentrations. **b** The atomic volume mismatch between solutes and Mg. The change of **c** the Twist-prpr2 velocity and **d** the TB velocity with shear modulus ratio and atomic volume mismatch. From dark blue to red, the facet velocity changes from small to large. The size of markers changes with the atomic volume of solute elements.

solutes, the solute effect on facet motion is not sufficient while for alloys with 10 at.% solutes, several solute elements have to be excluded, as the high solute concentration of these alloys results in alloy melting at 1.6 GPa shear stress, or the twin embryo growth is completely restricted at such concentration. In Figs. 14c, d, the velocities of Twist-prpr2 and TBs are plotted against the variation of the shear modulus ratio and the atomic volume mismatch. Figures 14c, d confirm that smaller atomic volume mismatches with Mg and smaller shear modulus contribute to faster facet motion, but they cannot fully explain the

behavior of every facet. For example, Ca and Ce have similar atomic volumes, and the alloys have similar shear moduli, yet the facet velocities in the two corresponding alloys are noticeably different. Moreover, the TB velocity in pure Mg is lower than in Mg-Li, Mg-Y, and Mg-Nd alloys. Other factors that likely affect facet velocities but have not been computed in this work include the disconnection nucleation energy and disconnection migration energy. Solutes can induce the formation of twinning disconnections (by reducing the disconnection nucleation energy) or inhibit the migration of twinning disconnections (by

increasing the disconnection migration energy) [36, 45, 68]. Similar solute effects are likely to apply to other disconnections formed on other twin facets, but such solute effects are not considered in Fig. 14d. We examined many alloy and element properties (such as the segregation energy, cohesive energy, or TB energy) and did not find conclusive trends. However, this does not imply that such properties do not contribute to twin facet velocities, yet a conclusive correlation has not been identified. Future work may collect and/or generate more relevant data and use techniques of machine learning to investigate the correlation between facet velocity and element/alloy properties.

We point out that like every numerical study, our simulations bear a number of limitations. Since a twin embryo was inserted into the initial configuration, the nucleation process of the twin and the alloying effect on twin nucleation is not considered. Also, the growth of a single twin embryo was studied, while the interaction of the twin embryo with other defects, such as lattice dislocations, vacancies, and other twins, was not considered. In practice, there are usually dislocations located at or near the boundaries of the twin [69–71], affecting twin growth. While two twins approach each other, their local stress fields also interact and alter the growth of each twin [72, 73]. In addition, the solute concentrations used in this work may exceed the maximum solubility limit of some Mg alloys, so second-phase particles are expected to be formed. Instead of introducing the second phase into the simulation, which inevitably raises the interfaces between the second phase and the matrix and requires discussions of particle size, shape, or separation distance, we focus on comparing the effect of different alloying elements per se with increasing composition, which amplifies the solute effect. Moreover, no solute segregation is considered in this work. Solute atoms are introduced by randomly replacing Mg atoms and forming solid solutions. Therefore, the solute concentration at the interface is the same as the bulk solute concentration and the global solute concentration. This could underestimate the interface solute concentration. However, twin embryo growth is fast compared to the typical relaxation times of solutes. In experiments, solute segregation can be manipulated by heat treatment, as shown in the work of Nie et al. [16], who studied the segregation of Gd and Zn to coherent TBs, comparing the mechanical performance of

two types of samples with and without annealing. Samples after annealing exhibited higher solute concentrations at coherent TBs and showed no discernible twin growth compared to samples without annealing. The segregation energy of various solutes to twin facets such as TB and BP/PBs was previously obtained by DFT or MD calculations [33–35]. A negative segregation energy means the interface energy is reduced by solutes occupying specific sites on the interface, and the corresponding segregated solutes exhibit a strong pinning effect on interface motion. By contrast, in this study, the positions of solutes are fixed throughout the simulation, and pinning occurs when a boundary passes through the solutes. Finally, the low simulation temperature is used to identify the disconnections formed on the different twin facets, while the temperature does affect the facet motion and twin growth [31], yet the temperature effect on twin growth in Mg alloys is out of the scope of this study.

We found both consistency and discrepancies between our findings and existing works. For example, Yu et al. [13] investigated the twinning behavior in Mg single crystals at the nanometer scale. They fabricated nanopillars with widths of 100–200 nm and thicknesses of 150 nm and loaded them in tension/compression and bending. For comparison, they also created "bulk samples" of significantly larger sizes. They managed to capture a few twin embryos in a bulk sample, viewed from the bright side. The twin thicknesses ranged from ∼ 4.3 to 5.5 nm, and the twin lengths ranged from ∼ 24.8 to ∼ 41.7 nm. The twin aspect ratios, calculated as twin lengths divided by twin thicknesses, hence ranged from 5.1 to 9.6. Our simulation results underestimate the twin aspect ratios, with a maximum value smaller than 3, due to the larger twin thicknesses obtained. One possible reason is the constant shear stresses maintained throughout our simulations, implying that once the global stresses are reduced by twin transformation, the simulation box is sheared further to return to the same stress level. In this case, once the applied stresses go beyond the threshold for twin growth, there is always sufficient driving force for twinning disconnections to be generated on horizontal TBs; hence, TBs can continue to migrate along the twin plane normal. Another possible reason is that we only consider the growth of a single twin embryo in our simulations, ignoring the effect of other defects, so that the solute

effect on facet motion can be isolated. By contrast, in the image provided by Yu et al. [13], the spacing between twins in bulk Mg ranged from ∼ 17.8 to 37.3 nm. Arul Kumar et al. [73] and El Kadiri et al. [74] reported that both parallel and intersecting twins could affect each other's growth by hardening twin thickening. The solute effect on twin–twin interactions or twin–dislocation interactions goes beyond the scope of this study and is an interesting point for future research.

Twin boundary and twin tip (referred to as f-TB) velocities measured during the deformation of Mg single crystals were reported by Kannan et al. [64], who showed that the TB and twin tip velocities vary with time, with peak values of ∼ 30 m s^{-1} and 1300 ± 300 m s^{-1}, respectively. Our results show no discernable growth of the bright side of the twin below 1.4 GPa, while from 1.4 to 1.6 GPa, the TB velocity ranges from 190 to 440 m s^{-1}, and the f-TB velocity from 510 to 750 m s^{-1}. Again, our results show a much higher TB velocity, similar to the overestimation of the twin thickness along the Z-axis. Yet more important than the quantitative data, both our work and Kannan et al. [64] show that the metrics associated with twin dynamics, such as twin extensions or facet velocities, cannot be treated as constant values, and it is hard to compare the data from different sources without knowing the stress/strain or growth stage at which twin thickness, aspect ratio or facet velocities are obtained. This makes a comparison with experimental data challenging.

The solute effect on twinning has also been investigated experimentally [4, 37]. Wang et al. [37] reported the increased critical resolved shear stress for twin nucleation and growth in Mg–Al alloys. They created Mg–Al micropillars and loaded them in compression (along the $[01\bar{1}0]$-direction). In this way, $\{10\bar{1}2\}$ tension twins dominate at the beginning of the pillar deformation, followed by large activation of basal slip. More importantly, due to the limited number of twins formed during the twinning-dominated deformation, the authors managed to identify the twin nucleation and growth stages from the stress–strain curves and determined the critical resolved shear stress for the two processes. The observation of higher critical resolved shear stresses for twin growth is consistent with our results that Al suppresses the overall twin growth at all three tested concentrations. The work of Stanford et al. [4] on the

twinning behavior in Mg-Y showed that the twin volume fraction decreases as the Y concentration increases, in contrast to our observation that Y slightly promotes twin growth. However, as discussed earlier, this is an example of how hard it is to isolate the twin nucleation process from the twin growth process. Therefore, it is impossible to determine whether Y atoms harden twin nucleation, twin growth, or both. Wang calculated the energy associated with twin nucleation and growth in Mg-Y alloys, using methods of MD and first principles, but obtained inconsistent results [75]. MD simulations with a MEAM potential [76] showed a slight increase in the energy barrier for twin growth in Mg-1 at.% Y, Mg-2 at.% Y, and Mg-3 at.% Y, while DFT calculations on Mg-1.56 at.% Y showed a decrease in the energy barrier [68]. More rigorous studies should be conducted to give a convincing conclusion. The twin facet kinetics obtained in this work inspires in situ experiments on twin growth in Mg alloys and can be used to validate simulations at larger length scales, e.g., using the phase field method.

Conclusions

Molecular dynamics simulations were performed to study 3D twin embryo growth in pure Mg as well as a variety of alloys (Mg–Al, Mg–Zn, Mg–Sn, Mg–Y, Mg–Pb, Mg–Ca, Mg–Li, Mg–Ce, and Mg–Nd). Our simulation results reveal the following:

- Alloying Mg with Al, Zn, Pb, or Li atoms decreases the lattice constant, while adding Sn, Y, Ce, Ca, or Nd increases the lattice constant. Al, Pb, and Sn atoms help increase the shear modulus, while Y, Ce, Ca, Li, Zn, or Nd decrease the shear modulus.
- Both the simulations on pure Mg and Mg–X alloys reveal that the motion of the dark side of the twin embryo is faster than that of the bright side, with Twist-prpr2 facets being the fastest facets.
- Alloying Mg with all studied solutes reduces the velocities of facets on the dark side of the twin embryo. The higher the solute concentration, the stronger the pinning effect of the solute elements. While for facets on the bright side, particularly TBs, the majority of solutes promote facet motion. As the solute concentration increases, the pinning

effect of solutes becomes dominant, and there are fewer solute species that can promote TB motion.

- Y and Li atoms do not significantly change facet motion as the solute concentration increases.
- Solutes Li, Y, Ce, and Nd show the opposite effect on the motion of facets on the dark and bright sides, i.e., they reduce the velocity of facets on the dark side while enhancing the velocity of facets on the bright side. Consequently, the velocity difference between facets such as TBs and Twist-prpr2 decreases. Even though solutes Al, Zn, Pb, Ca, and Sn reduce the velocity of both TBs and Twist-prpr2 facets, most of them can still decrease the velocity difference of these two facets.
- The evolution of the twin atomic fraction with time shows that Y and Li (at all three tested concentrations) and 4 at.% of Nd enhance the growth of the twin embryo.
- The change of solute/Mg potential energy with time shows that Sn must overcome the largest energy barrier as the lattice changes from the matrix to the twin, and this causes a strong pinning effect of Sn on twin facet motion.
- Larger shear modulus and larger atomic volume mismatch correlate with lower facet velocities, yet these two factors cannot fully explain the twinning behavior in all tested alloys. The latter is an outcome of various factors, possibly including the disconnection nucleation/migration energies and Mg-X bond energies, which require future studies.

In summary, our work provides atomic scale information on the early stages of twin embryo growth in Mg-X alloys. The solute effects on twin facet motion, especially the Twist-pypy1, Tilt-pypy1, and Twist-prpr2 facets that were observed only recently, are reported for the first time. These findings may contribute to designing Mg-based alloys with desired properties.

Acknowledgements

Funding

Supplementary Information: The online version contains supplementary material available at https://doi.org/10.1007/s10853-023-08263-3.

References

[1] Jayasathyakawin S, Ravichandran M, Baskar N et al (2020) Mechanical properties and applications of magnesium alloy: review. Mater Today Proc 27:909–913. https://doi.org/10.1016/j.matpr.2020.01.255

[2] Prasad SVS, Prasad SB, Verma K et al (2022) The role and significance of magnesium in modern day research: a review. J Magnes Alloys 10:1–61. https://doi.org/10.1016/j.jma.2021.05.012

[3] Choi S, Shin E, SEONG B, (2007) Simulation of deformation twins and deformation texture in an AZ31 Mg alloy under uniaxial compression. Acta Mater 55:4181–4192. https://doi.org/10.1016/j.actamat.2007.03.015

[4] Stanford N, Marceau RKW, Barnett MR (2015) The effect of high yttrium solute concentration on the twinning behaviour of magnesium alloys. Acta Mater 82:447–456. https://doi.org/10.1016/j.actamat.2014.09.022

[5] Christian JW, Mahajan S (1995) Deformation twinning. Prog Mater Sci 39:1–157. https://doi.org/10.1016/0079-6425(94)00007-7

[6] Reed-Hill RE, Robertson WD (1957) Additional modes of deformation twinning in magnesium. Acta Metall 5:717–727. https://doi.org/10.1016/0001-6160(57)90074-3

[7] Hutchinson WB, Barnett MR (2010) Effective values of critical resolved shear stress for slip in polycrystalline magnesium and other hcp metals. Scr Mater 63:737–740. https://doi.org/10.1016/j.scriptamat.2010.05.047

[8] Sánchez-Martín R, Pérez-Prado MT, Segurado J et al (2014) Measuring the critical resolved shear stresses in Mg alloys by instrumented nanoindentation. Acta Mater 71:283–292. https://doi.org/10.1016/j.actamat.2014.03.014

[9] Xie KY, Alam Z, Caffee A, Hemker KJ (2016) Pyramidal I slip in c-axis compressed Mg single crystals. Scr Mater 112:75–78. https://doi.org/10.1016/j.scriptamat.2015.09.016

[10] Chen L, Ye T, Wang Y et al (2021) Development of mechanical properties in AZ31 magnesium alloy processed by cold dynamic extrusion. Mater Charact 182:111535. https://doi.org/10.1016/j.matchar.2021.111535

[11] Wang X, Jiang L, Cooper C et al (2020) Toughening magnesium with gradient twin meshes. Acta Mater 195:468–481. https://doi.org/10.1016/j.actamat.2020.05.021

[12] Gong M, Hirth JP, Liu Y et al (2017) Interface structures and twinning mechanisms of twins in hexagonal metals. Mater Res Lett 5:449–464. https://doi.org/10.1080/21663831.2017.1336496

[13] Yu Q, Qi L, Chen K et al (2012) The nanostructured origin of deformation twinning. Nano Lett 12:887–892. https://doi.org/10.1021/nl203937t

[14] Yu Q, Wang J, Jiang Y et al (2014) Twin–twin interactions in magnesium. Acta Mater 77:28–42. https://doi.org/10.1016/j.actamat.2014.05.030

[15] Yu Q, Wang J, Jiang Y et al (2014) Co-zone $\{10\bar{1}2\}$ twin interaction in magnesium single crystal. Mater Res Lett 2:82–88. https://doi.org/10.1080/21663831.2013.867291

[16] Nie JF, Zhu YM, Liu JZ, Fang XY (2013) (2013) Periodic segregation of solute atoms in fully coherent twin boundaries. Science (1979) 340:957–960. https://doi.org/10.1126/science.1229369

[17] Tu J, Zhang X, Wang J et al (2013) Structural characterization of $\{10\bar{1}2\}$ twin boundaries in cobalt. Appl Phys Lett 103:051903. https://doi.org/10.1063/1.4817180

[18] Braisaz T, Ruterana P, Nouet G (1997) Twin tip defects related to the nucleation and growth mechanisms of the twin $\{10\bar{1}2\}$ in zinc characterized by high-resolution electron microscopy. Philos Mag A 76:63–84. https://doi.org/10.1080/01418619708209962

[19] Lay S, Nouet G (1995) Morphology of (01·2) twins in zinc and related interfacial defects. Philos Mag A 72:603–617. https://doi.org/10.1080/01418619508243788

[20] Sun Q, Zhang XY, Ren Y et al (2014) Interfacial structure of $\{10\bar{1}2\}$ twin tip in deformed magnesium alloy. Scr Mater 90–91:41–44. https://doi.org/10.1016/j.scriptamat.2014.07.012

[21] Wang J, Yadav SK, Hirth JP et al (2013) Pure-shuffle nucleation of deformation twins in hexagonal-close-packed metals. Mater Res Lett 1:126–132. https://doi.org/10.1080/21663831.2013.792019

[22] Xu B, Capolungo L, Rodney D (2013) On the importance of prismatic/basal interfaces in the growth of twins in hexagonal close packed crystals. Scr Mater 68:901–904. https://doi.org/10.1016/j.scriptamat.2013.02.023

[23] Pond RC, Serra A, Bacon DJ (1999) Dislocations in interfaces in the h.c.p. metals—II. mechanisms of defect mobility under stress. Acta Mater 47:1441–1453. https://doi.org/10.1016/S1359-6454(99)00017-8

[24] Serra A, Bacon DJ (1996) A new model for $\{10\bar{1}2\}$ twin growth in hcp metals. Philos Mag A 73:333–343. https://doi.org/10.1080/01418619608244386

[25] Serra A, Bacon DJ, Pond RC (2002) Twins as barriers to basal slip in hexagonal-close-packed metals. Metall and Mater Trans A 33:809–812. https://doi.org/10.1007/s11661-002-1012-6

[26] Barrett CD, el Kadiri H (2014) The roles of grain boundary dislocations and disclinations in the nucleation of $\{10\bar{1}2\}$ twinning. Acta Mater 63:1–15. https://doi.org/10.1016/j.actamat.2013.09.012

[27] Zu Q, Tang X-Z, Xu S, Guo Y-F (2017) Atomistic study of nucleation and migration of the basal/prismatic interfaces in Mg single crystals. Acta Mater 130:310–318. https://doi.org/10.1016/j.actamat.2017.03.035

[28] Liu Y, Li N, Shao S et al (2016) Characterizing the boundary lateral to the shear direction of deformation twins in magnesium. Nat Commun 7:11577. https://doi.org/10.1038/ncomms11577

[29] Fernández A, Jérusalem A, Gutiérrez-Urrutia I, Pérez-Prado MT (2013) Three-dimensional investigation of grain boundary–twin interactions in a Mg AZ31 alloy by electron backscatter diffraction and continuum modeling. Acta Mater 61:7679–7692. https://doi.org/10.1016/j.actamat.2013.09.005

[30] Wang S, Gong M, McCabe RJ et al (2020) Characteristic boundaries associated with three-dimensional twins in hexagonal metals. Sci Adv 6:1–8. https://doi.org/10.1126/sciadv.aaz2600

[31] Gong M, Graham J, Taupin V, Capolungo L (2021) The effects of stress, temperature and facet structure on growth of $\{10\bar{1}2\}$ twins in Mg: a molecular dynamics and phase field study. Acta Mater 208:116603. https://doi.org/10.1016/j.actamat.2020.116603

[32] Wang X, Hu Y, Yu K et al (2022) Room temperature deformation-induced solute segregation and its impact on twin boundary mobility in a Mg-Y alloy. Scr Mater 209:114375. https://doi.org/10.1016/j.scriptamat.2021.114375

[33] Zhang J, Dou Y, Zheng Y (2014) Twin-boundary segregation energies and solute-diffusion activation enthalpies in Mg-based binary systems: a first-principles study. Scr Mater 80:17–20. https://doi.org/10.1016/j.scriptamat.2014.02.004

[34] Huang Z, Nie JF (2021) Interaction between hydrogen and solute atoms in $\{10\bar{1}2\}$ twin boundary and its impact on boundary cohesion in magnesium. Acta Mater 214:117009. https://doi.org/10.1016/j.actamat.2021.117009

[35] Huang Z, Turlo V, Wang X et al (2021) Dislocation-induced Y segregation at basal-prismatic interfaces in Mg. Comput Mater Sci 188:11024. https://doi.org/10.1016/j.commatsci.2020.110241

[36] Yi P, Falk ML (2019) Thermally activated twin thickening and solute softening in magnesium alloys: a molecular simulation study. Scr Mater 162:195–199. https://doi.org/10.1016/j.scriptamat.2018.11.021

[37] Wang J, Molina-Aldareguía JM, Lorca JL (2020) Effect of Al content on the critical resolved shear stress for twin nucleation and growth in Mg alloys. Acta Mater 188:215–227. https://doi.org/10.1016/j.actamat.2020.02.006

[38] He C, Li Z, Chen H et al (2021) Unusual solute segregation phenomenon in coherent twin boundaries. Nat Commun 12:722. https://doi.org/10.1038/s41467-021-21104-8

[39] Hantzsche K, Bohlen J, Wendt J et al (2010) Effect of rare earth additions on microstructure and texture development of magnesium alloy sheets. Scr Mater 63:725–730. https://doi.org/10.1016/j.scriptamat.2009.12.033

[40] Dong H, Pan F, Jiang B et al (2015) Mechanical properties and deformation behaviors of hexagonal Mg–Li alloys. Mater Des 1980–2015(65):42–49. https://doi.org/10.1016/j.matdes.2014.08.033

[41] Wan YJ, Zeng Y, Zeng Q et al (2021) Simultaneously improved strength and toughness of a Mg–Sn alloy through abundant prismatic lath-shaped precipitates. Mater Sci Eng, A 811:141087. https://doi.org/10.1016/j.msea.2021.141087

[42] Dang K, Tomé CN, Capolungo L (2021) The $\{10\bar{1}2\}$ non-cozone twin-twin interactions in Mg: a stability and mobility study using 3-D atomistic simulations. Scr Mater 200:113913. https://doi.org/10.1016/j.scriptamat.2021.113913

[43] Gong M, Liu G, Wang J et al (2018) Atomistic simulations of interaction between basal <a> dislocations and three-dimensional twins in magnesium. Acta Mater 155:187–198. https://doi.org/10.1016/j.actamat.2018.05.066

[44] Wan X, Zhang J, Mo X, Pan F (2019) 3D atomic-scale growth characteristics of $\{10\bar{1}2\}$ twin in magnesium. J Magnes Alloys 7:474–486. https://doi.org/10.1016/j.jma.2019.05.002

[45] Ghazisaeidi M, Hector LG, Curtin WA (2014) Solute strengthening of twinning dislocations in Mg alloys. Acta Mater 80:278–287. https://doi.org/10.1016/j.actamat.2014.07.045

[46] Beyerlein IJ, Zhang X, Misra A (2014) Growth twins and deformation twins in metals. Annu Rev Mater Res 44:329–363. https://doi.org/10.1146/annurev-matsci-070813-113304

[47] Niezgoda SR, Kanjarla AK, Beyerlein IJ, Tomé CN (2014) Stochastic modeling of twin nucleation in polycrystals: An application in hexagonal close-packed metals. Int J Plast 56:119–138. https://doi.org/10.1016/j.ijplas.2013.11.005

[48] Knezevic M, Daymond MR, Beyerlein IJ (2016) Modeling discrete twin lamellae in a microstructural framework. Scr Mater 121:84–88. https://doi.org/10.1016/j.scriptamat.2016.04.026

[49] Plimpton S (1995) Fast parallel algorithms for short-range molecular dynamics. J Comput Phys 117:1–19. https://doi.org/10.1006/jcph.1995.1039

[50] Bae GT, Bae JH, Kang DH et al (2009) Effect of Ca addition on microstructure of twin-roll cast AZ31 Mg alloy. Met Mater Int 15:1–5. https://doi.org/10.1007/s12540-009-0001-3

[51] Singh C, Narayan RL, Jain J (2021) Influence of simultaneous alloying with Ca and Sc on the high temperature deformation mechanism, texture, and recrystallization behavior of Mg-Ca-Sc alloys. Mater Charact 179:111343. https://doi.org/10.1016/j.matchar.2021.111343

[52] Kim Y-M, Kim NJ, Lee B-J (2009) Atomistic modeling of pure Mg and Mg–Al systems. Calphad 33:650–657. https://doi.org/10.1016/j.calphad.2009.07.004

[53] Kim Y-M, Jung I-H, Lee B-J (2012) Atomistic modeling of pure Li and Mg–Li system. Model Simul Mat Sci Eng 20:035005. https://doi.org/10.1088/0965-0393/20/3/035005

[54] Kim K-H, Jeon JB, Lee B-J (2015) Modified embedded-atom method interatomic potentials for Mg–X (X=Y, Sn, Ca) binary systems. Calphad 48:27–34. https://doi.org/10.1016/j.calphad.2014.10.001

[55] Kim K-H, Lee B-J (2017) Modified embedded-atom method interatomic potentials for Mg-Nd and Mg-Pb binary systems. Calphad 57:55–61. https://doi.org/10.1016/j.calphad.2017.03.003

[56] Jang H-S, Seol D, Lee B-J (2021) Modified embedded-atom method interatomic potentials for Mg–Al–Ca and Mg–Al–Zn ternary systems. J Magnes Alloys 9:317–335. https://doi.org/10.1016/j.jma.2020.09.006

[57] Lee J-K, Lee B-J (2021) The origin of activation of non-basal slip in Mg-Ce dilute alloy: an atomistic simulation study. Metall and Mater Trans A 52:964–974. https://doi.org/10.1007/s11661-020-06128-x

[58] Stukowski A (2010) Visualization and analysis of atomistic simulation data with OVITO–the open visualization tool. Model Simul Mat Sci Eng 18:015012. https://doi.org/10.1088/0965-0393/18/1/015012

[59] Larsen PM, Schmidt S, Schiøtz J (2016) Robust structural identification via polyhedral template matching. Model Simul Mat Sci Eng 24:055007. https://doi.org/10.1088/0965-0393/24/5/055007

[60] Hu Y, Turlo V, Beyerlein IJ et al (2020) Disconnection-mediated twin embryo growth in Mg. Acta Mater 194:437–451. https://doi.org/10.1016/j.actamat.2020.04.010

[61] He Y, Li B, Wang C, Mao SX (2020) Direct observation of dual-step twinning nucleation in hexagonal close-packed crystals. Nat Commun 11:2483. https://doi.org/10.1038/s41467-020-16351-0

[62] Long TR, Smith CS (1957) Single-crystal elastic constants of magnesium and magnesium alloys. Acta Metall 5:200–207. https://doi.org/10.1016/0001-6160(57)90166-9

[63] Gumbsch P, Gao H (1999) Dislocations faster than the speed of sound. Science (1979) 283:965–968. https://doi.org/10.1126/science.283.5404.965

[64] Kannan V, Hazeli K, Ramesh KT (2018) The mechanics of dynamic twinning in single crystal magnesium. J Mech Phys Solids 120:154–178. https://doi.org/10.1016/j.jmps.2018.03.010

[65] Jia Y, Jiang S, Tan J et al (2022) The evolution of local stress during deformation twinning in a Mg-Gd-Y-Zn alloy. Acta Mater 222:117452. https://doi.org/10.1016/j.actamat.2021.117452

[66] Arul Kumar M, Kanjarla AK, Niezgoda SR et al (2015) Numerical study of the stress state of a deformation twin in magnesium. Acta Mater 84:349–358. https://doi.org/10.1016/j.actamat.2014.10.048

[67] Arul Kumar M, Clausen B, Capolungo L et al (2018) Deformation twinning and grain partitioning in a hexagonal close-packed magnesium alloy. Nat Commun 9:4761. https://doi.org/10.1038/s41467-018-07028-w

[68] Luque A, Ghazisaeidi M, Curtin WA (2014) A new mechanism for twin growth in Mg alloys. Acta Mater 81:442–456. https://doi.org/10.1016/j.actamat.2014.08.052

[69] Khosravani A, Fullwood DT, Adams BL et al (2015) Nucleation and propagation of $\{10\bar{1}2\}$ twins in AZ31 magnesium alloy. Acta Mater 100:202–214. https://doi.org/10.1016/j.actamat.2015.08.024

[70] Yaddanapudi K, Leu B, Kumar MA et al (2021) Accommodation and formation of $\{10\bar{1}2\}$ twins in Mg-Y alloys. Acta Mater 204:116514. https://doi.org/10.1016/j.actamat.2020.116514

[71] Wang F, Agnew SR (2016) Dislocation transmutation by tension twinning in magnesium alloy AZ31. Int J Plast 81:63–86. https://doi.org/10.1016/j.ijplas.2016.01.012

[72] Arul Kumar M, Gong M, Beyerlein IJ et al (2019) Role of local stresses on co-zone twin-twin junction formation in HCP magnesium. Acta Mater 168:353–361. https://doi.org/10.1016/j.actamat.2019.02.037

[73] Arul Kumar M, Beyerlein IJ, Tomé CN (2016) Effect of local stress fields on twin characteristics in HCP metals. Acta Mater 116:143–154. https://doi.org/10.1016/j.actamat.2016.06.042

[74] El Kadiri H, Kapil J, Oppedal AL et al (2013) The effect of twin–twin interactions on the nucleation and propagation of twinning in magnesium. Acta Mater 61:3549–3563. https://doi.org/10.1016/j.actamat.2013.02.030

[75] Wang FX (2019) Energetics calculation of $\{10\bar{1}2\}$ Twin nucleation and growth in magnesium and alloys using density functional theory and atomistic simulation. PhD Dissertation. University of Nevada, Reno

[76] Ahmad R, Groh S, Ghazisaeidi M, Curtin WA (2018) Modified embedded-atom method interatomic potential for Mg-Y alloys. Model Simul Mat Sci Eng 26:065010. https://doi.org/10.1088/1361-651X/aacfd2